Sellar and Parasellar Masses

3

Gitanjali V. Patel, Sasan Karimi, and Robert J. Young

Lesions located within the sella and parasellar region of the brain may present with similar clinical symptoms and imaging findings. Anatomic location and key imaging characteristics can aid in the differentiation of these tumors. Major anatomic references within the sella and parasellar region include the pituitary gland, pituitary stalk, optic chiasm, hypothalamus, cavernous sinus, sphenoid sinus, and the meninges. Although the most common tumors located within this region are pituitary adenoma, it is important to consider other less common entities that will also be discussed in this chapter [1]. Normal pituitary may vary in size with gender and age. Premenopausal women tend to have a larger pituitary gland than men and postmenopausal women [1, 2]. Magnetic resonance imaging (MRI) is generally the modality of choice for identification of lesions within this region. There are a few imaging pitfalls and it is important to be aware that nearly 15–20 % of lesions found within the pituitary are asymptomatic incidental findings [2].

G.V. Patel
Department of Radiology, Memorial Sloan-Kettering Cancer Center, 1275 York Avenue, MRI-1156, New York, NY 10065, USA
e-mail: gita.patel@gmail.com

S. Karimi (✉) • R.J. Young
Department of Radiology,
New York Presbyterian Hospital/Weill Cornell Medical College, New York, NY, USA

Neuroradiology Service, Department of Radiology,
Memorial Sloan-Kettering Cancer Center,
1275 York Avenue, MRI-1156, New York, NY 10065, USA
e-mail: karimis@mskcc.org; youngr@mskcc.org

Pituitary Adenoma

Pituitary adenomas are benign tumors of the anterior pituitary that account for 10–15 % of all intracranial tumors [2]. These are the most common suprasellar masses found in adults. The majority occur in middle-aged females, with hyperfunctioning or secreting adenomas more likely to present earlier at a smaller size than nonfunctioning adenomas [3].

Pituitary Microadenoma

A microadenoma is ≤10 mm in diameter. Prolactin-secreting microadenomas are more common in patients 20–35 years old whereas microadenomas that secrete growth hormone are more common in patients 30–50 years old [4].

Microadenomas are commonly visualized as well-defined lesions that enhance less than the normal pituitary gland [4]. Dynamic contrast-enhanced MR may be useful as normal pituitary tissue normally enhances faster than microadenoma. Even when small, microadenomas may cause a mass effect that results in increased convexity of the superior margin of the pituitary gland or contralateral displacement of the infundibulum [4, 5].

S. Karimi (ed.), *Atlas of Brain and Spine Oncology Imaging*, Atlas of Oncology Imaging,
DOI 10.1007/978-1-4614-5653-7_3,

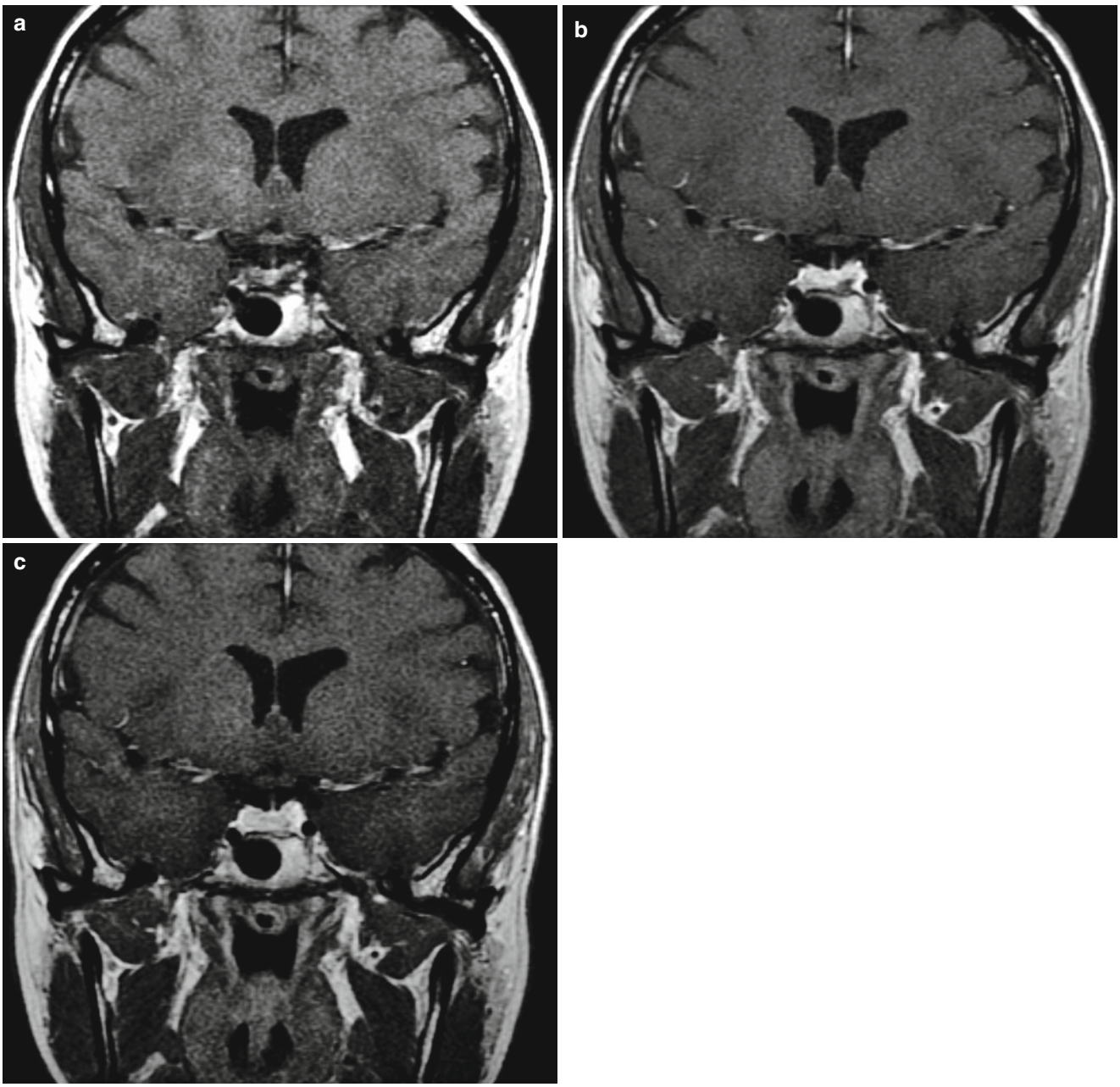

Fig. 3.1 Pituitary microadenoma. Pre-contrast (**a**), early dynamic contrast (**b**), and late dynamic contrast (**c**) coronal T1-weighted images show progressive enhancement of a microadenoma in the inferior left pituitary gland. The lesion is best seen on the early dynamic image; many microadenomas may be difficult to detect on routine non-dynamic contrast images when the differential enhancement has equalized with normal pituitary tissue

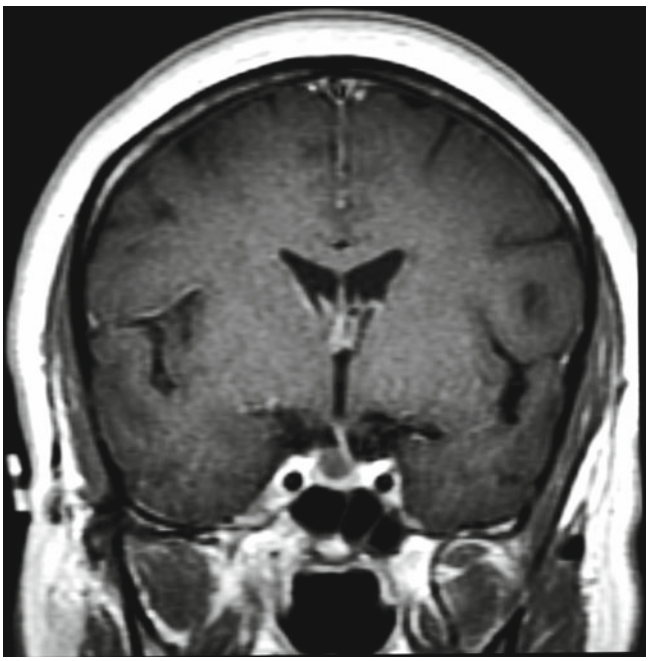

Fig. 3.2 Pituitary cyst. Coronal contrast T1-weighted image shows increased superior convexity of the right pituitary gland and contralateral displacement of the infundibulum by the nonenhancing right pituitary cyst that mimics a cystic microadenoma. Pathology only revealed acellular mucoid material

Pituitary Macroadenoma

A macroadenoma is larger than 10 mm in diameter [6, 14]. Macroadenomas may cause endocrine symptoms, or visual disturbances due to mass effect upon the optic chiasm or prechiasmatic optic nerves. Management of macroadenoma can vary from medical management to surgical resection, often through a trans-sphenoidal approach [7].

Macroadenomas are expansile masses that often grow superiorly into the suprasellar cistern. When large, they may impinge upon or compress the optic apparatus. Hemorrhagic, proteinaceous, and cystic changes may variably occur. Lateral growth in the cavernous sinus may limit otherwise curative surgical resection of these tumors [5, 6].

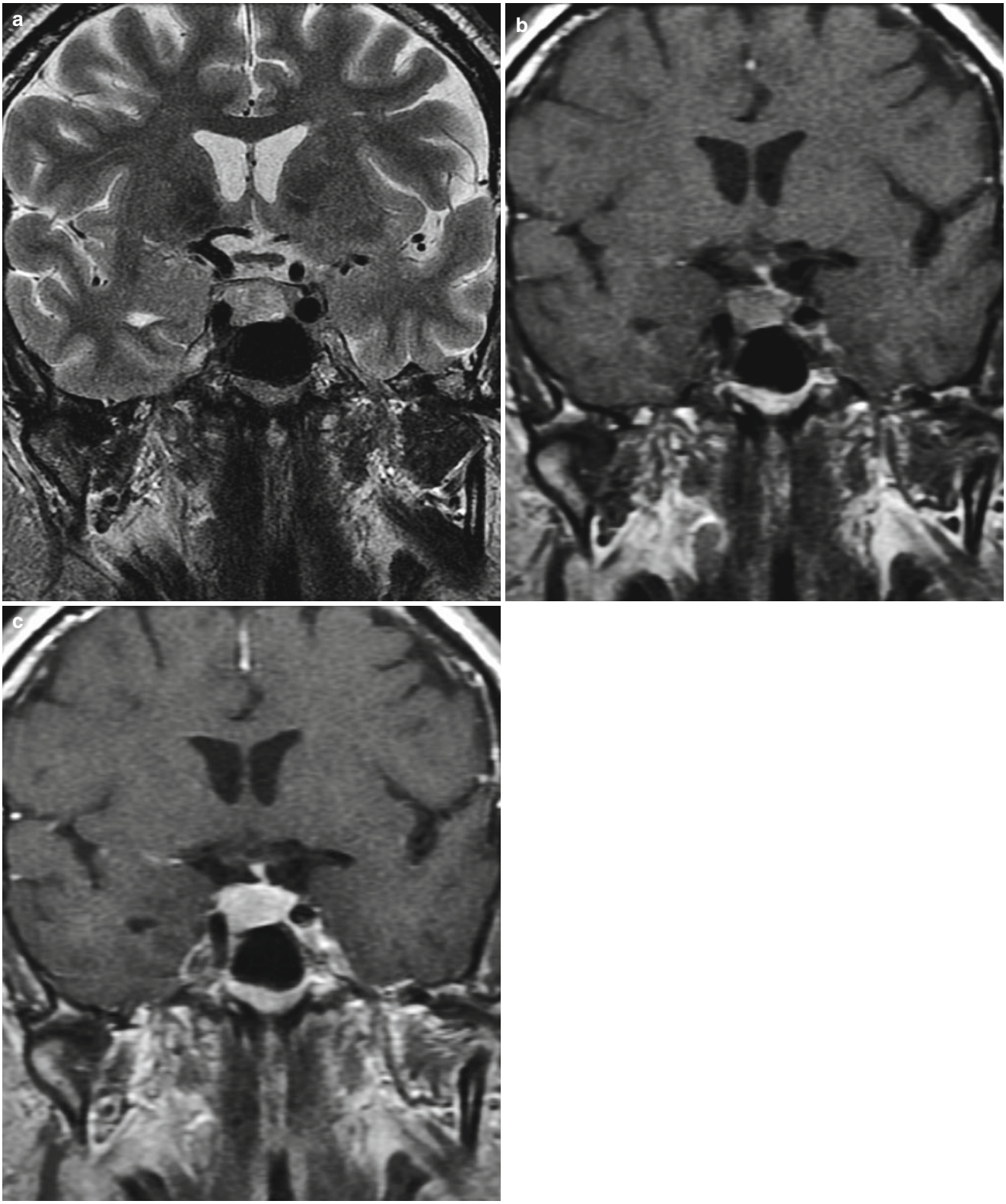

Fig. 3.3 Pituitary macroadenoma. Coronal T2-weighted (**a**) and early (**b**) and delayed (**c**) dynamic contrast T1-weighted images show a T2 hyperintense macroadenoma extending into the right cavernous sinus and displacing the infundibulum to the left. The macroadenoma is difficult to distinguish from normal pituitary tissue by the delayed image (**c**)

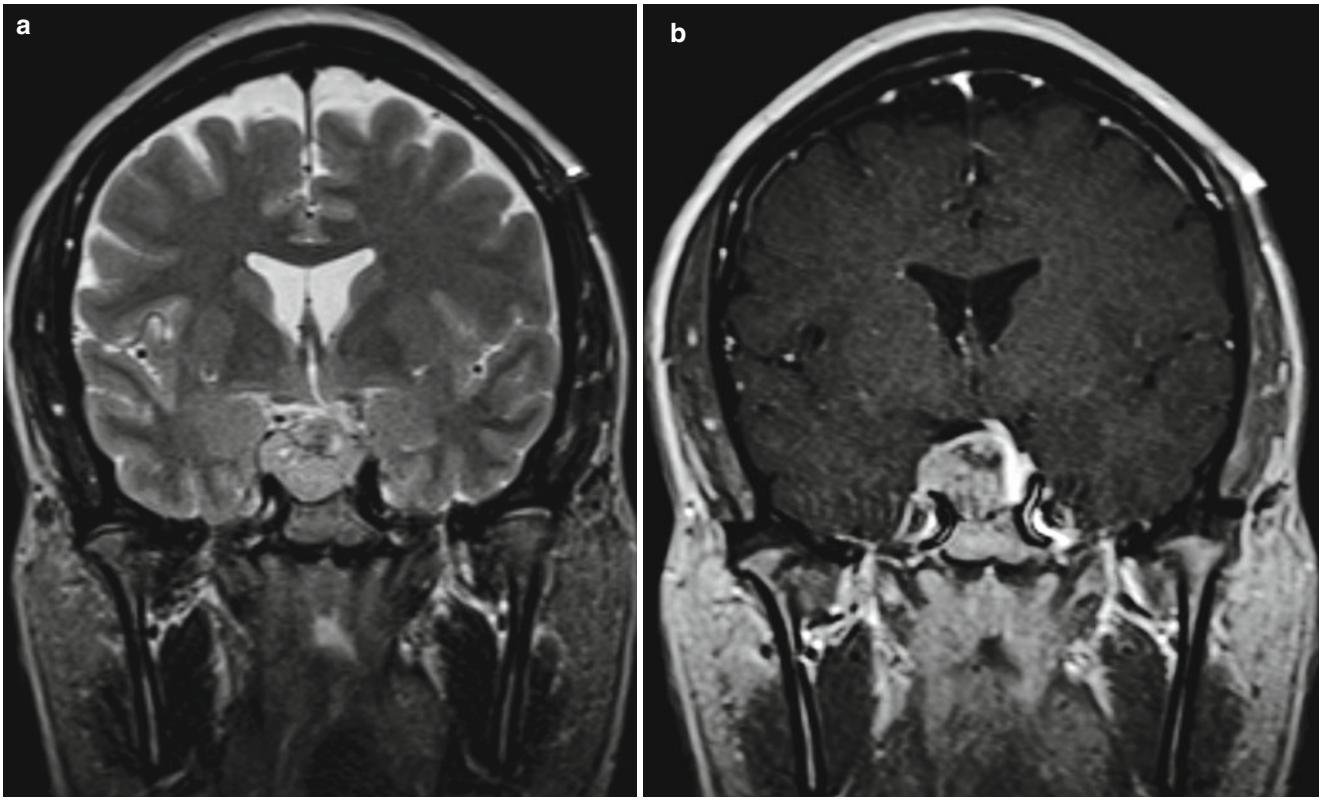

Fig. 3.4 Pituitary macroadenoma. Coronal T2-weighted (**a**) and contrast T1-weighted (**b**) images show a heterogeneously enhancing right pituitary macroadenoma invading into the right cavernous sinus, with suprasellar extension and contralateral displacement of the infundibulum. The macroadenoma is easier to distinguish from the normal, avidly enhancing pituitary gland in the left sella in (**b**)

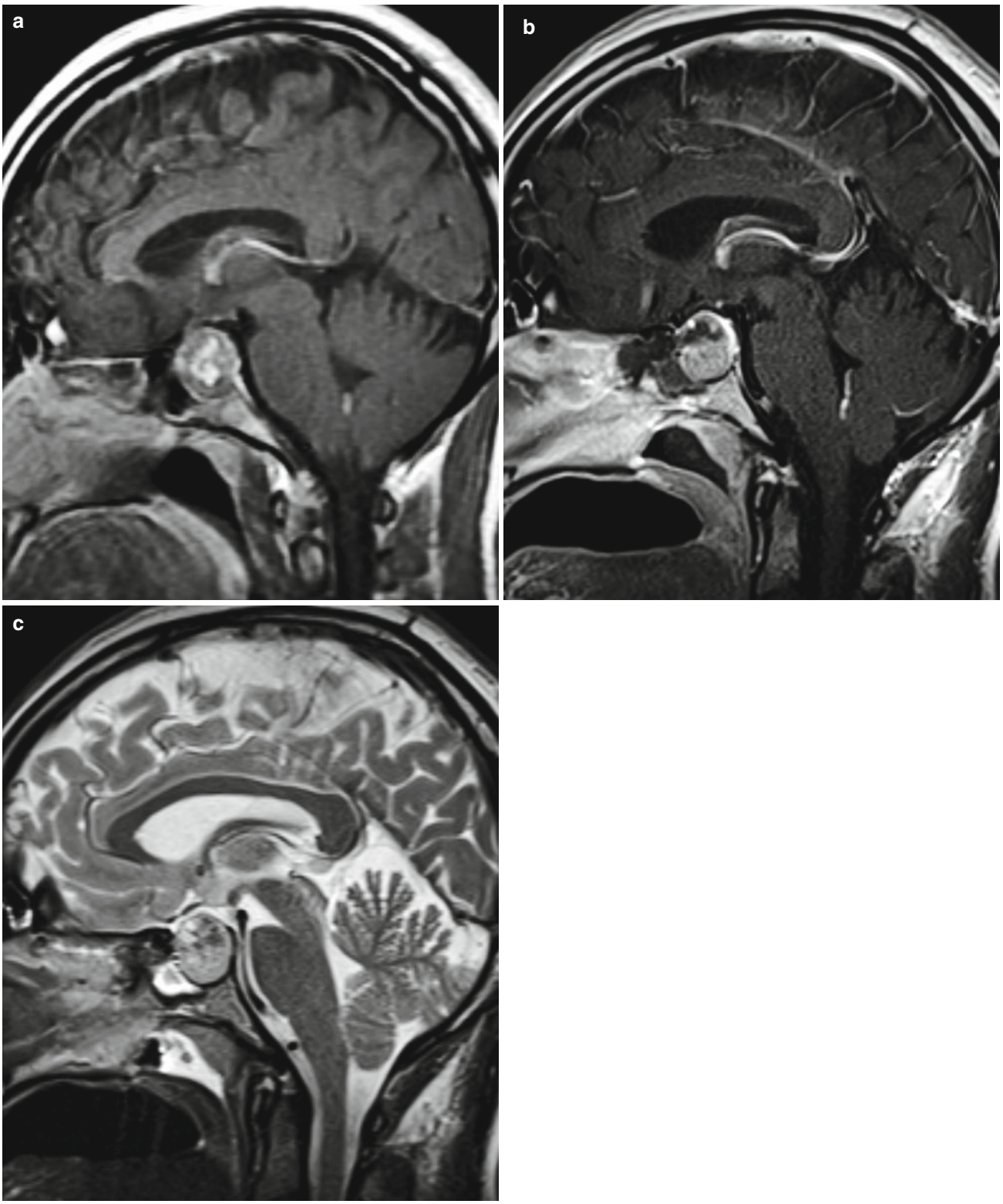

Fig. 3.5 Pituitary macroadenoma. Sagittal preoperative (**a**) and intraoperative (**b**) contrast T1-weighted images and intraoperative T2-weighted image (**c**) show subtotal resection of the macroadenoma extending into the suprasellar cistern. Curvilinear hyperintensity in (**a**) probably represents hemorrhagic and/or proteinaceous material within the macroadenoma

Invasive Pituitary Adenoma

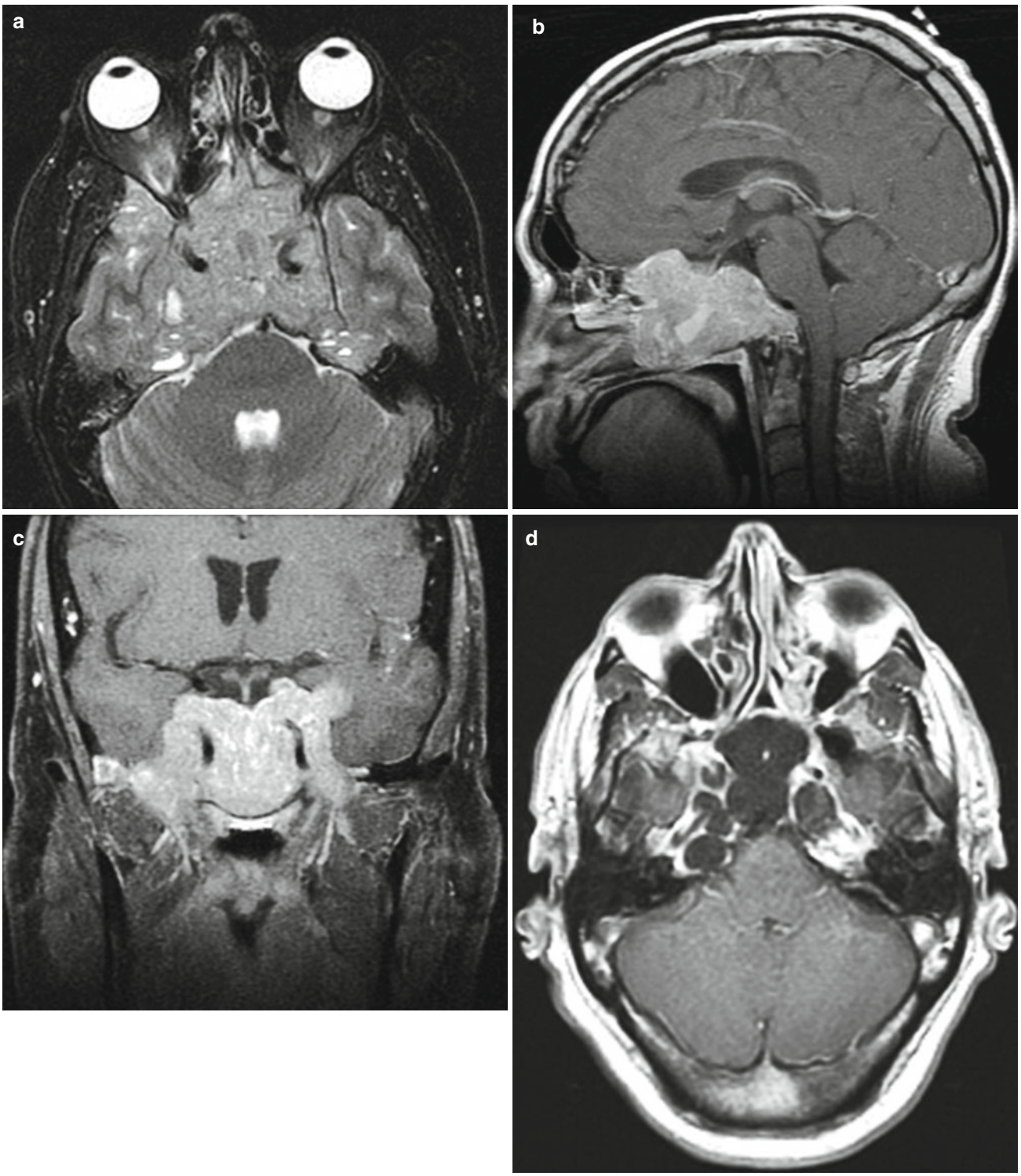

Fig. 3.6 Pretreatment axial T2 (**a**), sagittal T1 (**b**), and coronal T1 (**c**) post-contrast images of a patient with a large invasive pituitary adenoma infiltrating the central skull base. Small cystic changes are evident within the tumor on the axial T2-weighted image (**a**). Follow-up imaging 3 years after medical treatment demonstrates excellent treatment response as the mass has resolved leaving cystic and CSF-filled cavities with the skull base at sites of prior tumoral involvement. Axial (**d**) and sagittal T1 (**e**) post-contrast and coronal T2-weighted (**f**) images

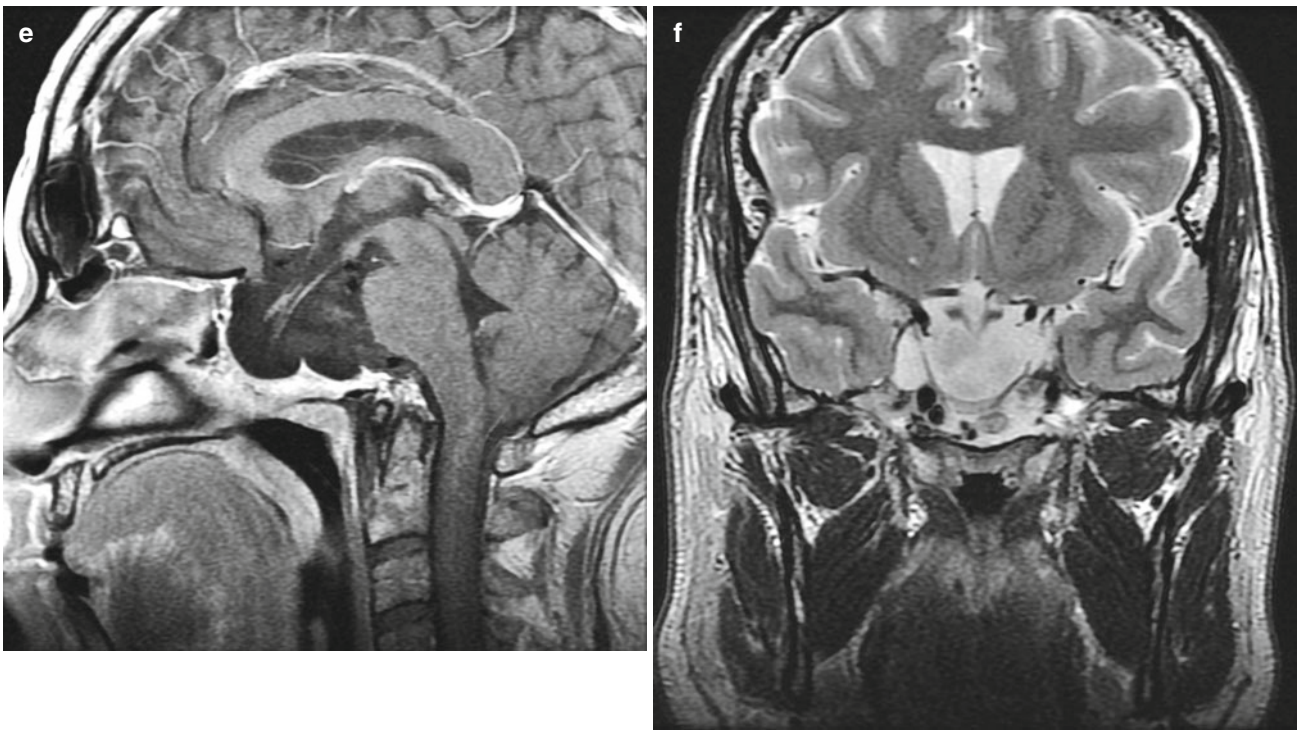

Fig. 3.6 (continued)

Rathke's Cleft Cyst

Rathke's cleft cyst (RCC) is a benign cyst that arises from the embryonic Rathke cleft. The cyst may contain a clear or mucoid material. RCCs are usually asymptomatic and are commonly found incidentally upon imaging or autopsy [8]. RCCs are most commonly diagnosed in the fifth decade of life and have a slight female predominance [9]. These cysts typically remain benign and management is usually conservative. If the patient is symptomatic aspiration or partial excision may be necessary.

Most RCCs are visualized as lobulated, well-defined, intrasellar, or suprasellar cysts that contain a small intracystic nodule [8]. More than 50 % of RCCs have a hypointense intracystic nodule upon T2-weighted imaging. RCCs typically do not enhance and rarely contain calcium. Around 40 % of these cysts are located completely within the sella and 60 % have suprasellar extension [9, 12].

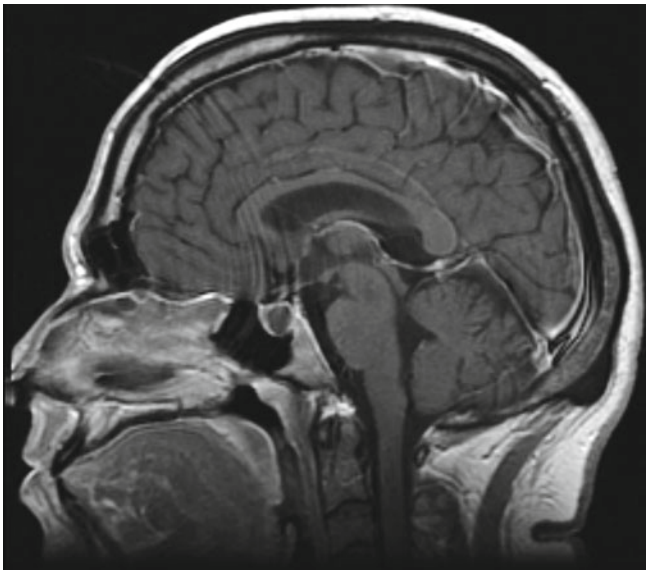

Fig. 3.7 Rathke cleft cyst. Sagittal contrast T1-weighted image shows a nonenhancing cystic lesion in the pituitary gland that could mimic a more common cystic pituitary adenoma. This RCC did not have the characteristic T1 hypointense, T2 hypointense intracystic nodule. Most craniopharyngiomas have cystic and solid-enhancing components (*see* "Craniopharyngioma")

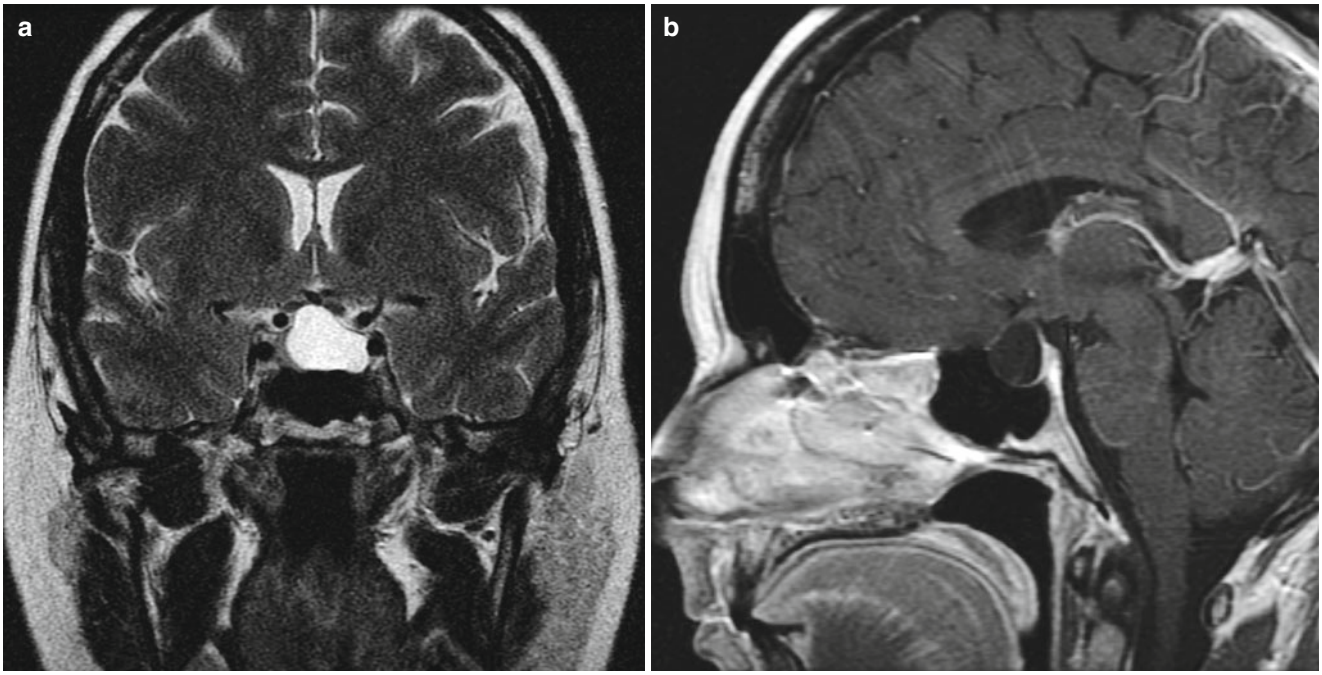

Fig. 3.8 Rathke cleft cyst. Coronal T2-weighted (**a**) and sagittal contrast T1-weighted (**b**) images demonstrate an expansile T2 hyperintense and T1 hypointense nonenhancing sellar and suprasellar lesion that impinges upon the prechiasmatic optic nerves. RCC fluid may show variable signal intensity; in this case, the fluid is slightly greater than normal cerebrospinal fluid on the T2-weighted image and equal on the T1-weighted image

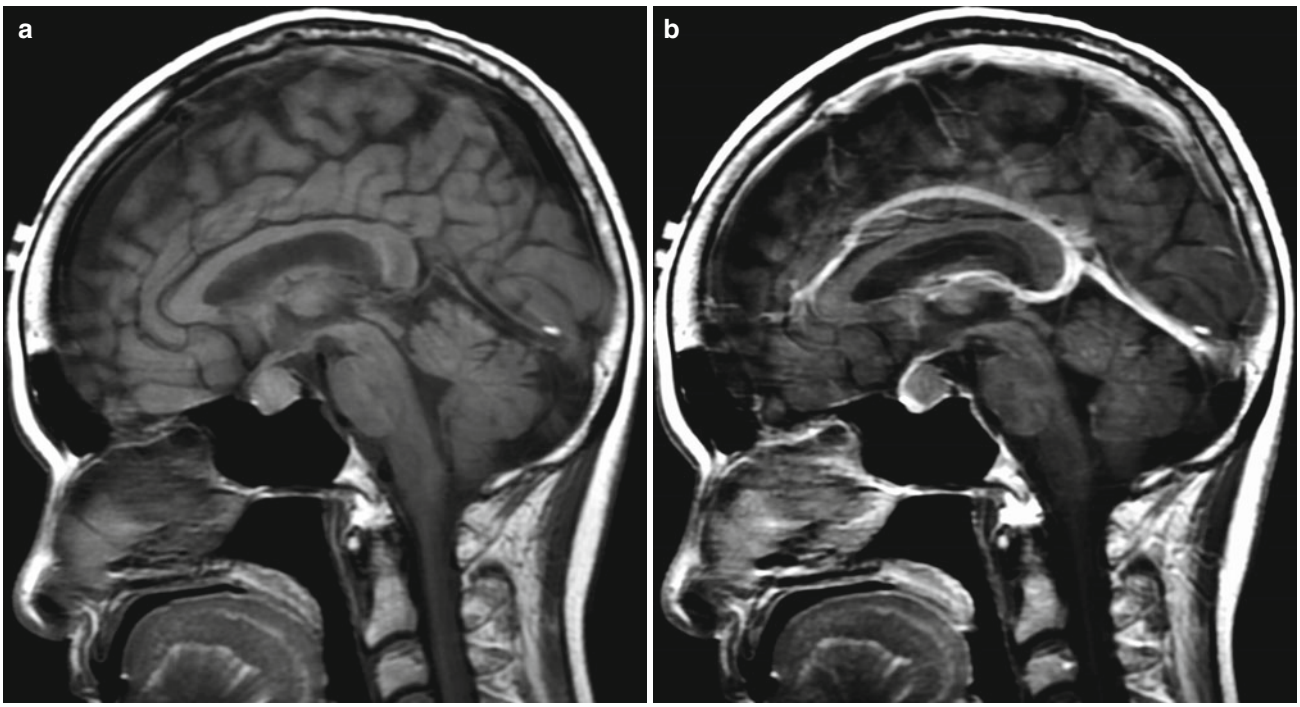

Fig. 3.9 Rathke cleft cyst. Sagittal T1-weighted images before (**a**) and after (**b**) contrast show a hyperintense, nonenhancing RCC

Craniopharyngioma

Craniopharyngioma are benign tumors that originate from embryonal cells originating from the Rathke cleft and/or craniopharyngeal duct epithelium [10]. This is the most common intracranial tumor in the pediatric population that is not of glial origin [11]. Craniopharyngiomas account for around half of all sellar tumors that occur in childhood [10]. This tumor type has no gender predominance and occurs in patients age 5–15 years old and patients older than age 50 [11]. Patients may present with visual and/or endocrine disturbances. Prognosis varies with tumor size; tumors with a diameter greater than 5 cm have a worse prognosis than tumors with diameters less than 5 cm [10].

Craniopharyngiomas are typically mixed solid and cystic lesions that contain calcium. Findings on pre-contrast T1-weighted MRI usually show a suprasellar lesion with high signal intensity [12]. These tumors may span to include the anterior, middle, and/or posterior cranial fossa. For surgical purposes, the location of the craniopharyngioma may be described as being sellar, prechiasmatic, or retrochiasmatic. Nonenhanced computed tomography (CT) may be useful to detect the presence of calcium if MR diagnosis is inconclusive [12].

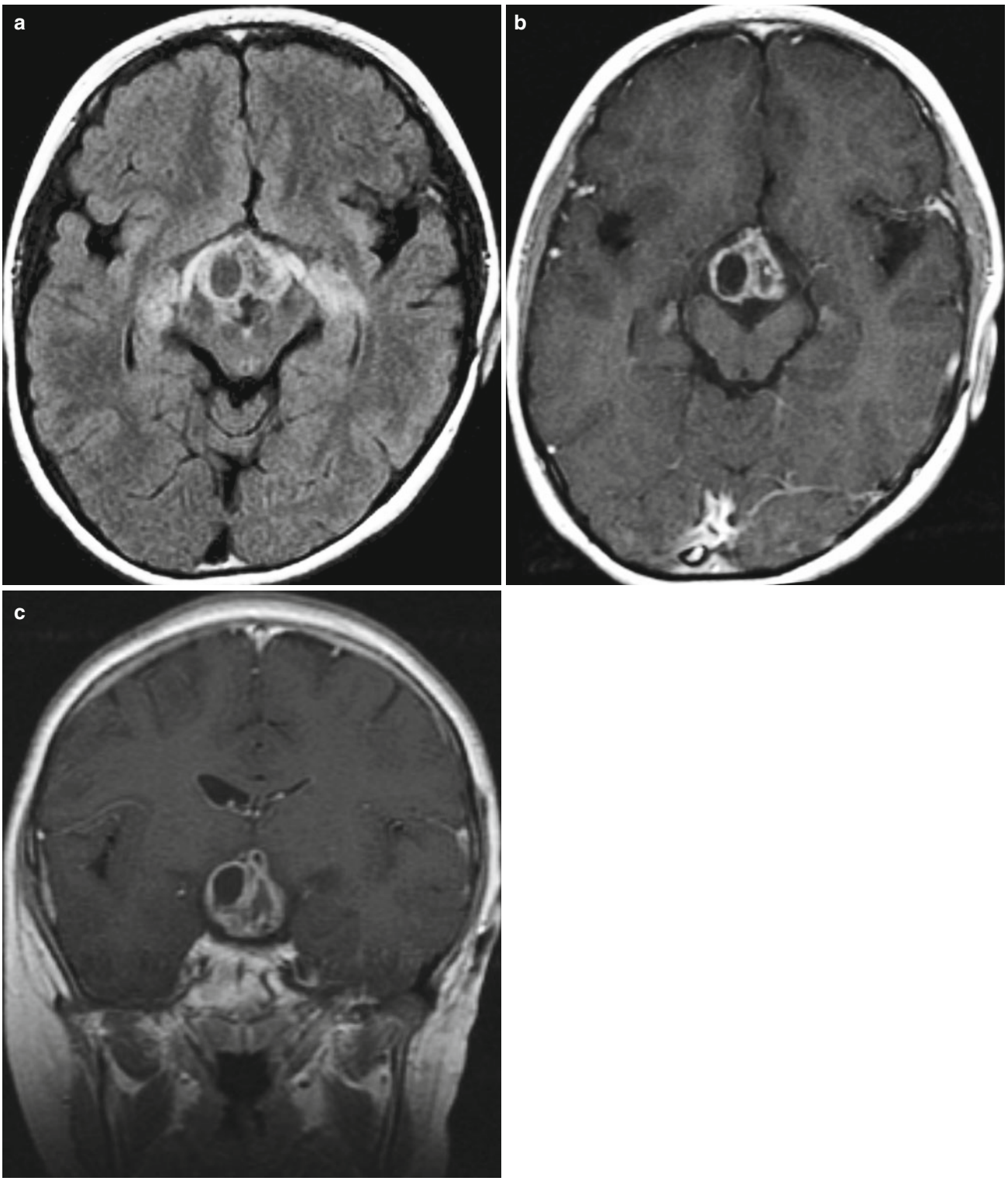

Fig. 3.10 Craniopharyngioma. Axial fluid attenuated inversion recovery (FLAIR) image (**a**) and axial (**b**) and coronal (**c**) contrast T1-weighted images show a solid and cystic suprasellar craniopharyngioma in a 7-year-old patient. Adjacent FLAIR hyperintense changes extend into the optic tracts and mesial temporal lobes (**a**)

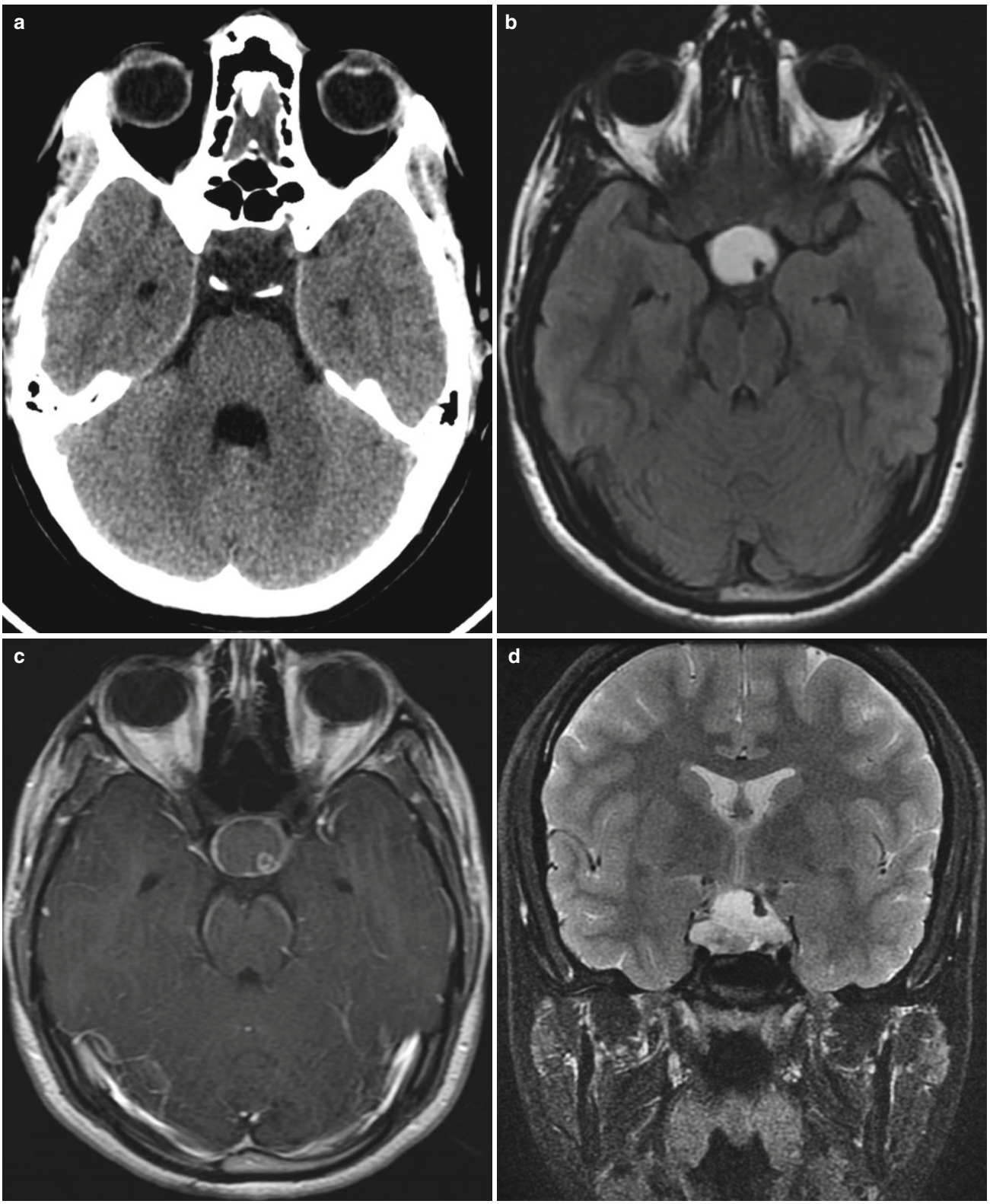

Fig. 3.11 Craniopharyngioma. Axial CT (**a**), axial FLAIR (**b**), and contrast T1-weighted (**c**) images and coronal T2-weighted image (**d**) reveal a T2/FLAIR hyperintense sellar and suprasellar adamantinomatous craniopharyngioma in a 16-year-old patient. There is lateral extension into the cavernous sinuses. The eccentric T2/FLAIR hypointense calcification and eccentric nodular enhancement are characteristic for adamantinomatous craniopharyngiomas compared to heterogeneously enhancing cystic pituitary macroadenomas (*see* "Pituitary Macroadenoma"). Adamantinomatous craniopharyngiomas peak in children at 5–14 years old

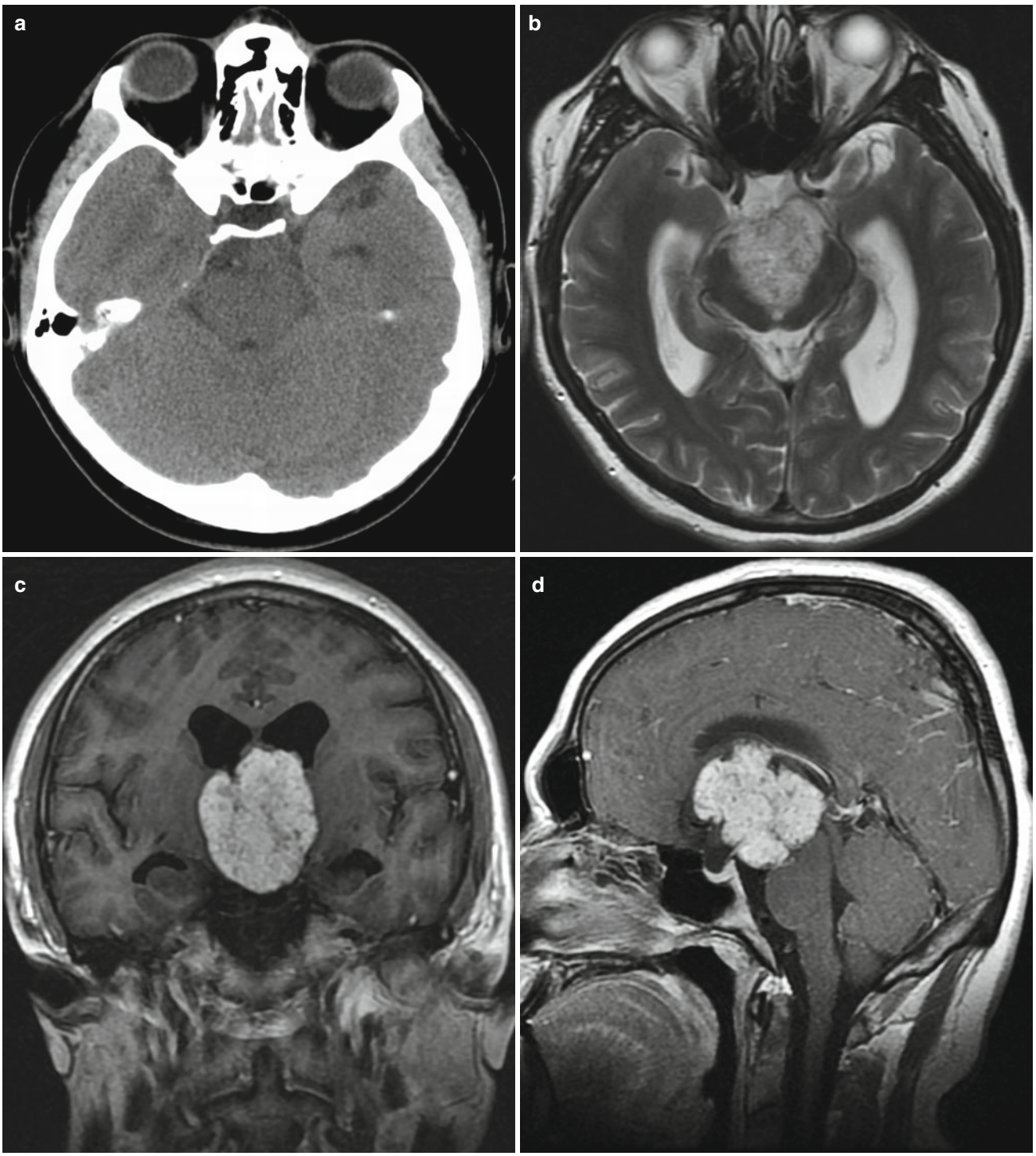

Fig. 3.12 Craniopharyngioma. Axial CT (**a**) and axial T2-weighted (**b**) images and coronal (**c**) and sagittal (**d**) contrast T1-weighted images show an expansile heterogeneously enhancing papillary craniopharyngioma in a 20-year-old patient. The tumor is centered in the suprasellar cistern and third ventricle, with splaying of the cerebral peduncles (**b**) and obstructive hydrocephalus manifest with dilatation of the lateral ventricles including the temporal horns. Squamous-papillary craniopharyngiomas are more common in adults at the smaller of the bimodal age peaks at 65–74 years old, and are more likely to be solid-enhancing compared to the solid and cystic adamantinomatous craniopharyngiomas in children

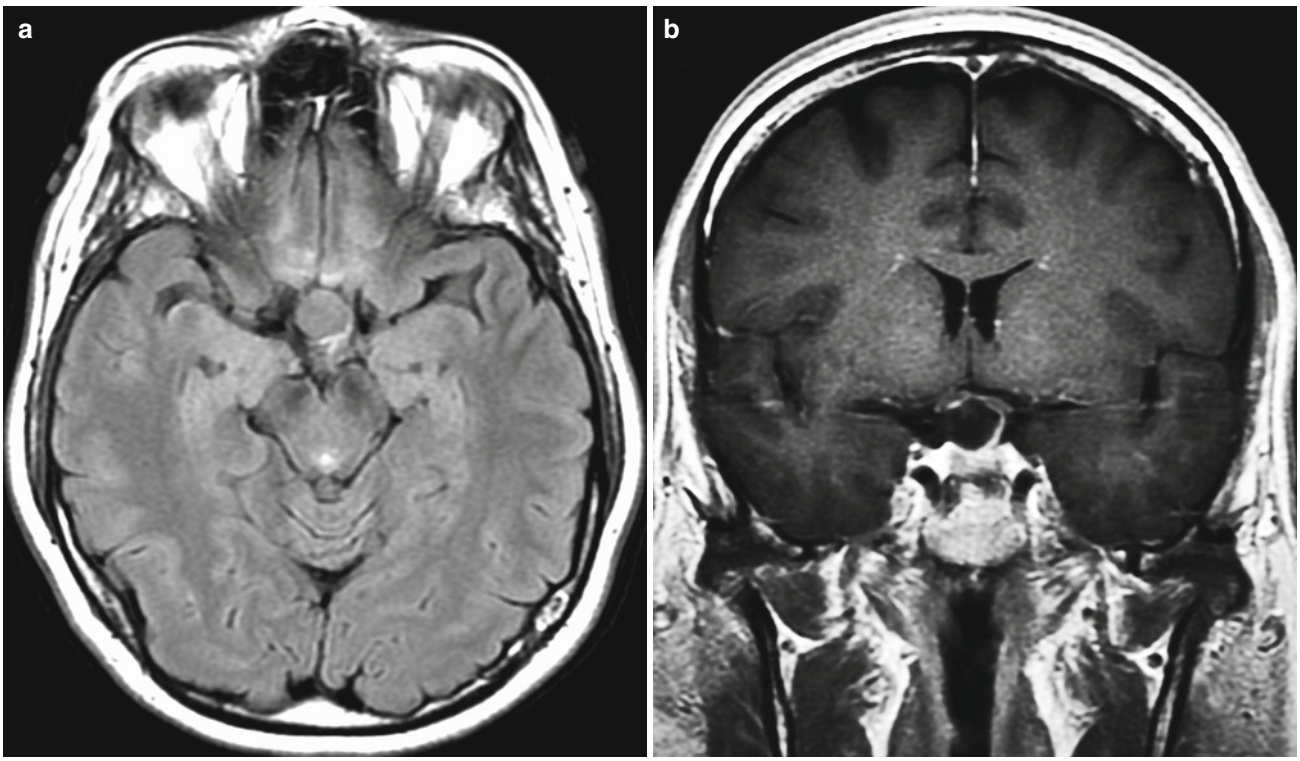

Fig. 3.13 Craniopharyngioma. Axial FLAIR (**a**) and coronal contrast T1-weighted (**b**) images show a cystic FLAIR hyperintense suprasellar adamantinomatous craniopharyngioma in a 49-year-old patient. These tumors are usually cystic and solid – the mild nodular peripheral enhancement along the superior margin adjacent to the right prechiasmatic optic nerve helps exclude a nonenhancing RCC (*see* "Rathke's Cleft Cyst"). The adamantinomatous subtype is more common in children

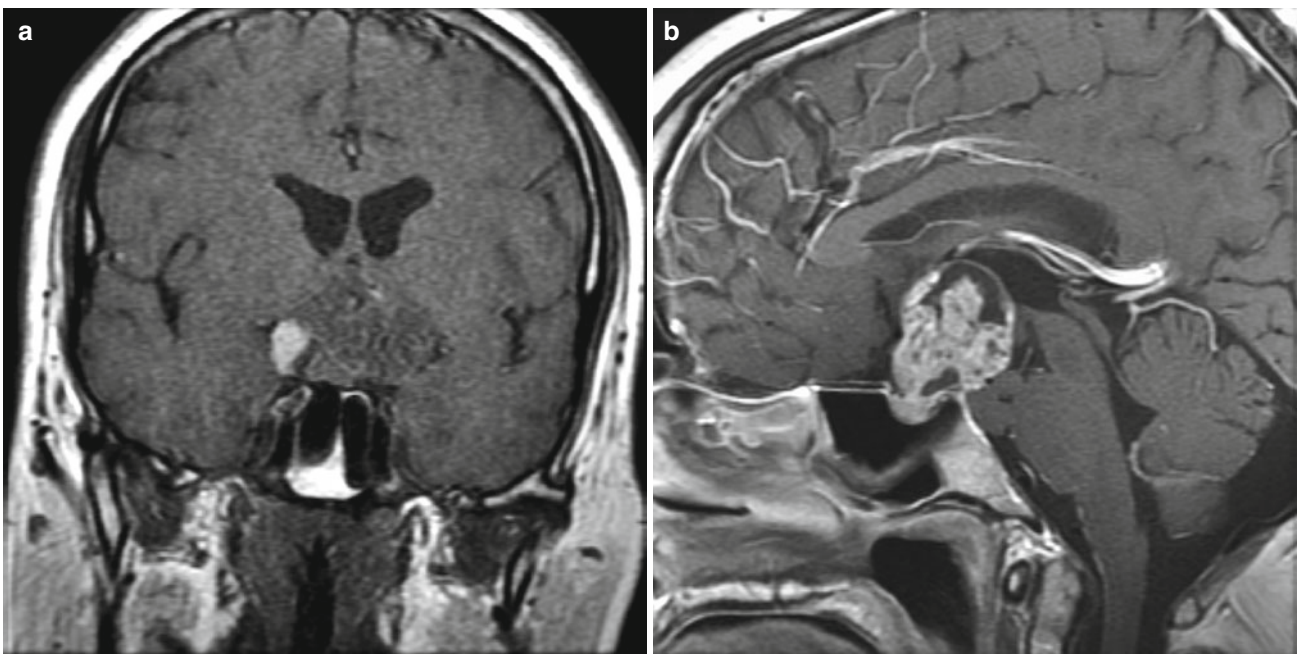

Fig. 3.14 Craniopharyngioma. Coronal (**a**) and contrast sagittal (**b**) T1-weighted images show a heterogeneously enhancing tumor centered in the suprasellar cistern with right eccentric pre-contrast T1 hyperintense blood products

Optic Pathway Glioma

Optic pathway gliomas are responsible for 5 % of all brain tumors. They comprise up to 15 % of supratentorial lesions within the pediatric population [13]. These are usually benign low-grade astrocytomas, although they are difficult to treat because of their location. In 10–20 % or more of patients with optic pathway gliomas, stigmata of neurofibromatosis type 1 are also found [13]. Compared to neurofibromatosis type 1–related tumors, sporadic optic pathway gliomas are more likely to have worse outcomes, impair vision, involve the optic chiasm, extend beyond the optic pathway, have larger size, and cystic nonenhancing components.

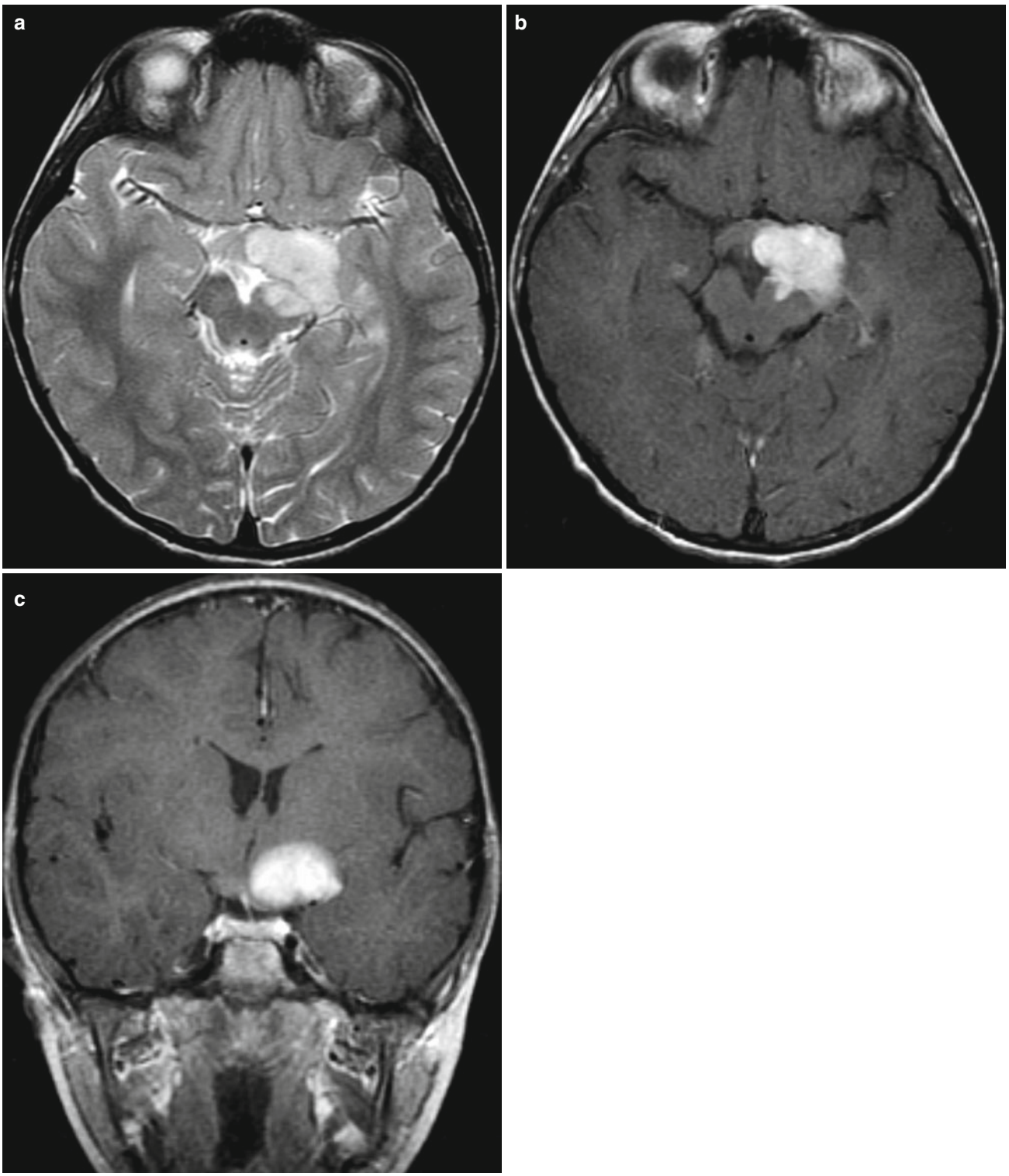

Fig. 3.15 Optic pathway glioma. Axial T2-weighted (**a**) and contrast axial (**b**) and coronal (**c**) T1-weighted images in a 4-year-old patient with a left optic chiasmatic-hypothalamic glioma. The expansile enhancing tumor extends posteriorly from the left optic chiasm along the optic tract and hypothalamus, inferiorly into the cerebral peduncle, and laterally into the mesial temporal lobe (*not shown*). Chiasmatic-hypothalamic gliomas in children younger than 5 years and older than 20 years old may demonstrate aggressive growth, despite the usually low-grade pathology. Posterior location may also indicate a poor outcome. This child received chemotherapy due to his age, tumor location, and slow growth over a year; radiation therapy is often deferred when possible in small children

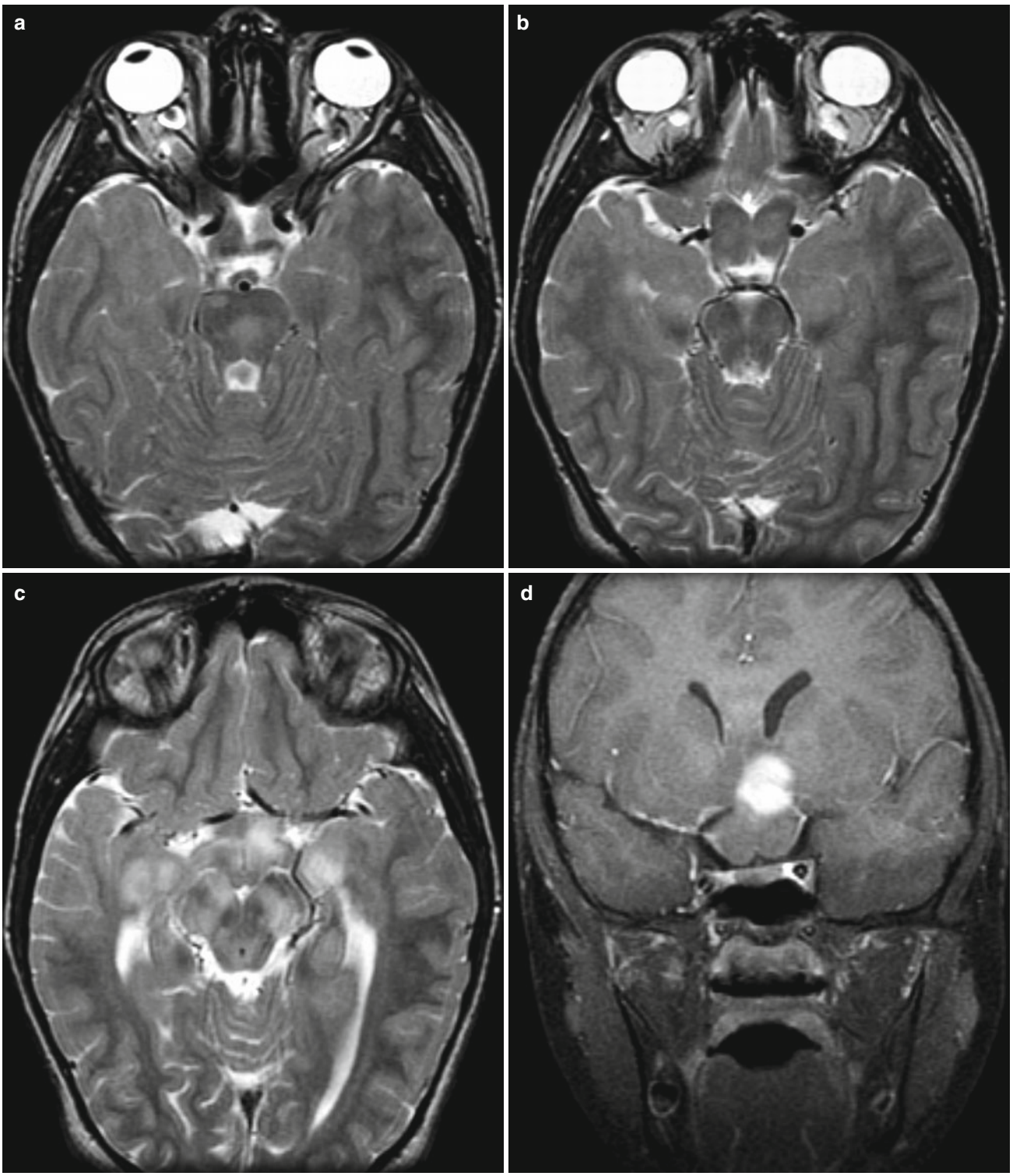

Fig. 3.16 Optic pathway glioma. Axial T2-weighted images (**a**–**c**) reveal expansile T2 hyperintense tumors in the prechiasmatic optic nerves (from anterior to posterior), chiasm, tracts, and pathways in a 7-year-old patient with bilateral chiasmatic-hypothalamic and optic pathway tumors. Additional areas of T2 hyperintensity in the brainstem and in the cerebral and cerebellar white matter (*not shown*) are consistent with vacuolar changes from underlying neurofibromatosis type 1. Coronal contrast fat-saturated T1-weighted image (**d**) 3 months later showed progression manifest by new enhancement in the optic chiasm and hypothalamus that prompted initiation of chemotherapy

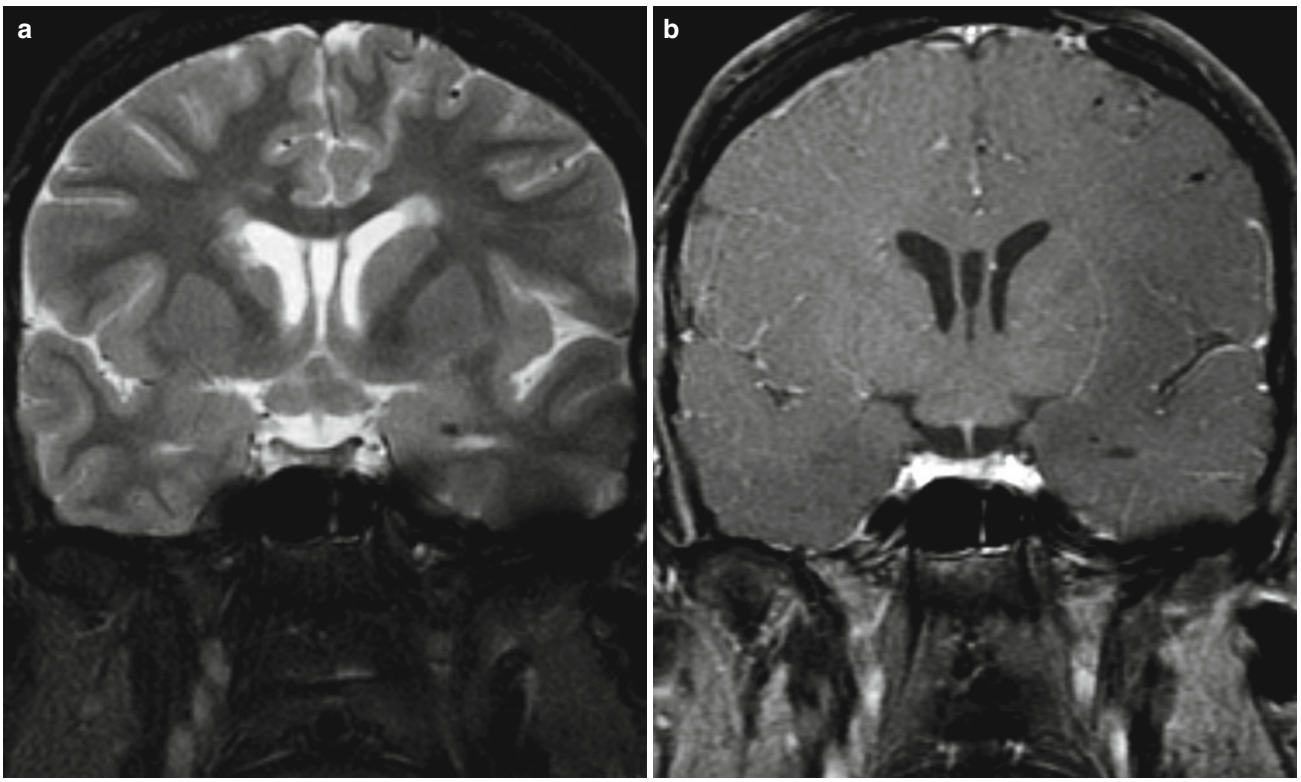

Fig. 3.17 Optic pathway glioma. Coronal fat-saturated T2-weighted (**a**) and contrast T1-weighted (**b**) images reveal an expansile nonenhancing glioma in the optic chiasm of a 19-year-old with neurofibromatosis type 1. Note the absence of normal internal carotid artery and proximal circle of Willis flow voids consistent with Moyamoya syndrome, one of many vascular lesions that may occur in neurofibromatosis type 1 (*see* Fig. 2.17a for normal arterial flow voids on a coronal T2-weighted image)

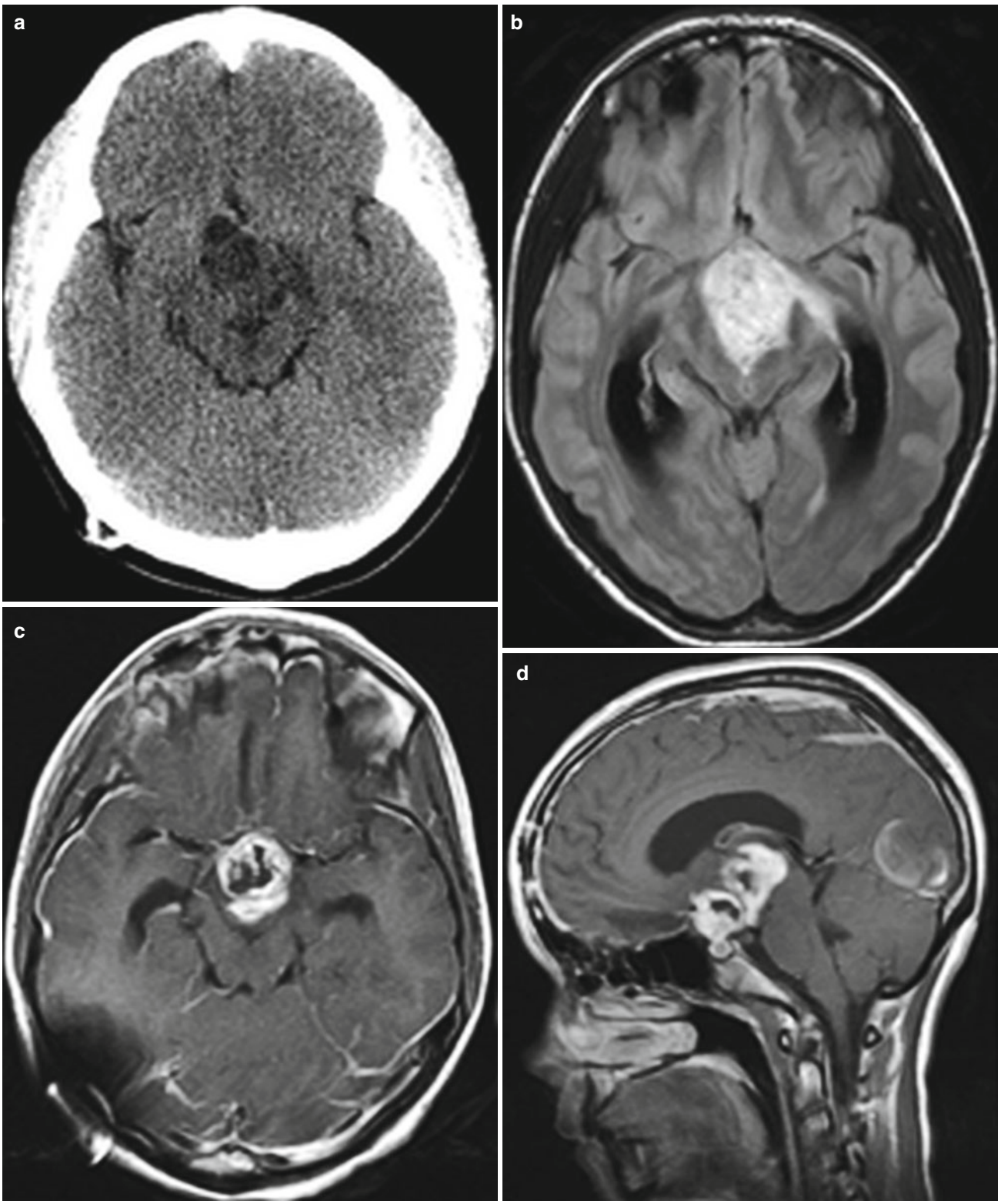

Fig. 3.18 Optic pathway glioma. Axial noncontrast CT (**a**), FLAIR (**b**), contrast axial (**c**), and sagittal (**d**) T1-weighted images and coronal T2-weighted image (**e**) reveal an expansile complex cystic and solid, heterogeneously enhancing mass lesion in the region of the optic chiasm, hypothalamus, and optic tracts. Mass effect from the tumor compresses the third ventricle, causing obstructive hydrocephalus with dilatation of the lateral ventricles including the temporal horns

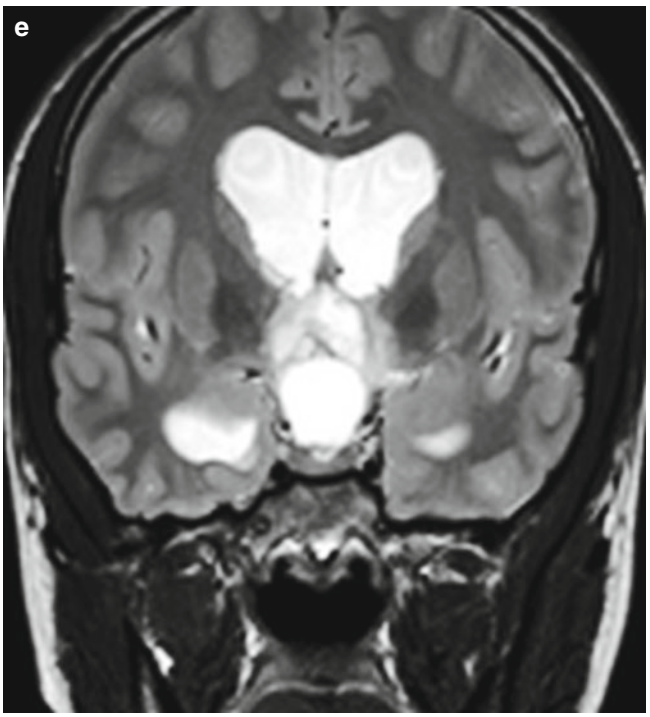

Fig. 3.18 (continued)

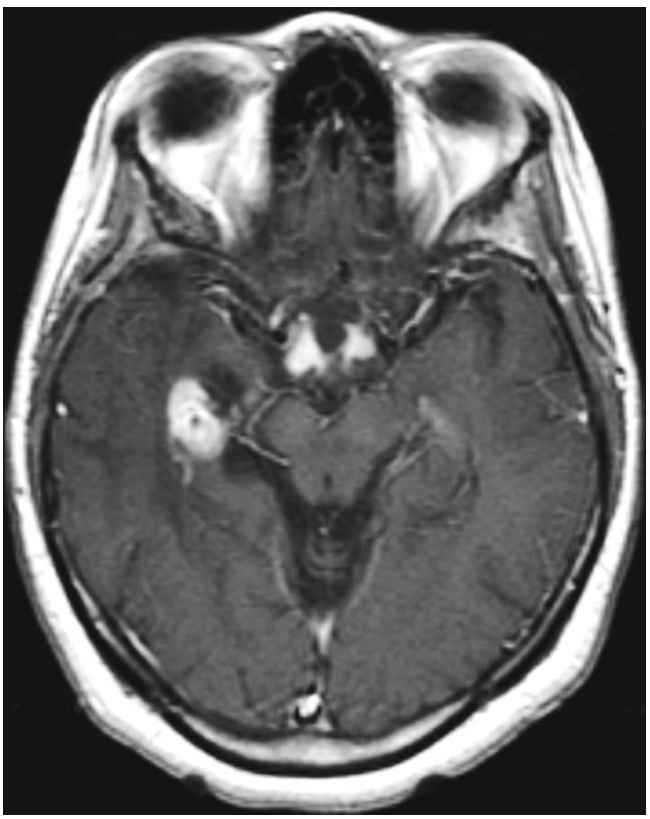

Fig. 3.19 Optic pathway glioma. Axial contrast T1-weighted image shows enhancing tumors in the bilateral optic tracts and in the right mesial temporal lobe near the lateral geniculate nucleus. Contiguous lesions were also present in the optic chiasm and hypothalamus (*not shown*)

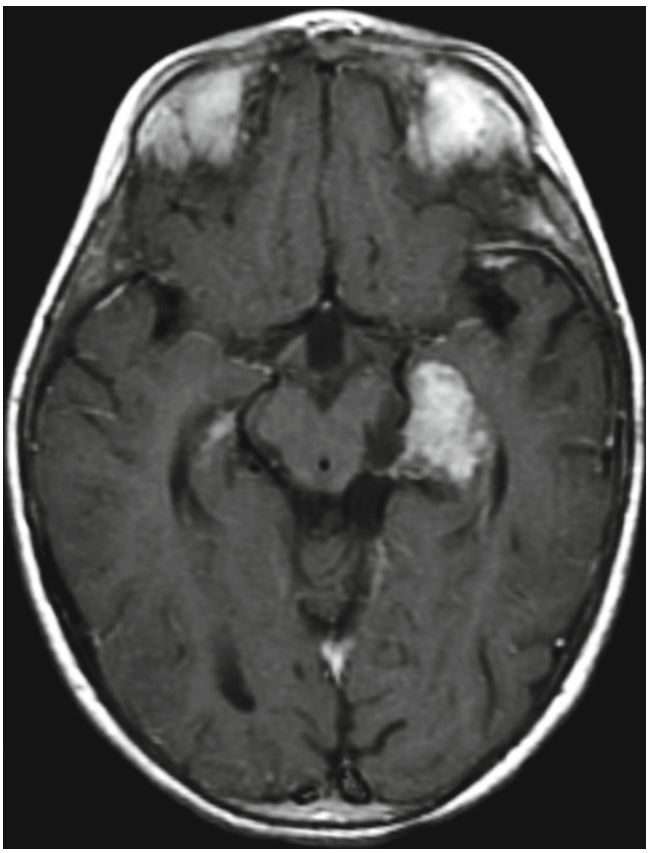

Fig. 3.20 Optic pathway glioma. Axial contrast T1-weighted image shows an enhancing tumor in the left mesial temporal lobe near the lateral geniculate nucleus with sparing of the remaining optic pathway

Pituitary Hypophysitis

Pituitary hypophysitis or autoimmune hypophysitis is visualized as radiographically similar to nonsecreting adenomas of the pituitary gland [14]. There are two histological subtypes of hypophysitis: lymphocytic and granulomatous [14]. Lymphocytic is the most commonly encountered subtype. Lymphocytic hypophysitis occurs most commonly in the female population with a 1:9 male:female ratio [15]. These lesions are often mistaken for adenomas, and are often diagnosed after subtotal resection and histologic correlation [14]. Pituitary hypophysitis is most commonly seen on MR as a thick, uniformly enhancing infundibulum with or without a pituitary mass lesion [14].

Fig. 3.21 Lymphocytic hypophysitis. Coronal contrast T1-weighted image shows thickening of the midline infundibulum to 0.5 cm with normal pituitary gland. In this postpartum 31-year-old woman who had developed diabetes insipidus with polydipsia and polyuria during her third trimester, the thickened infundibulum although nonspecific is consistent with pregnancy-related autoimmune lymphocytic hypophysitis. The infundibulum returned to a normal size (<3 mm) several months later

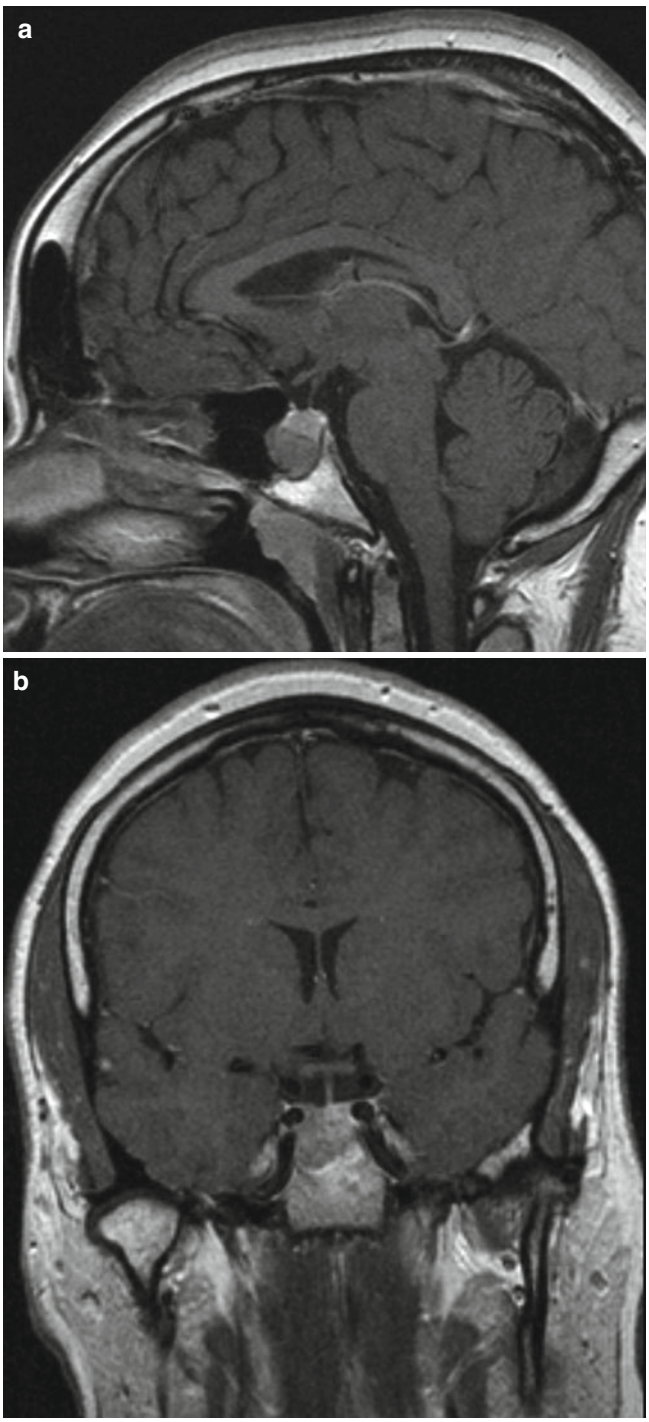

Fig. 3.22 Lymphocytic hypophysitis. Sagittal (**a**) and coronal (**b**) contrast T1-weighted images in a 25-year-old woman demonstrate an enhancing tumor in the sella that grows down into the sphenoid sinus. Pathology revealed a prolactin-expressing pituitary macroadenoma with coexisting lymphocytic hypophysitis

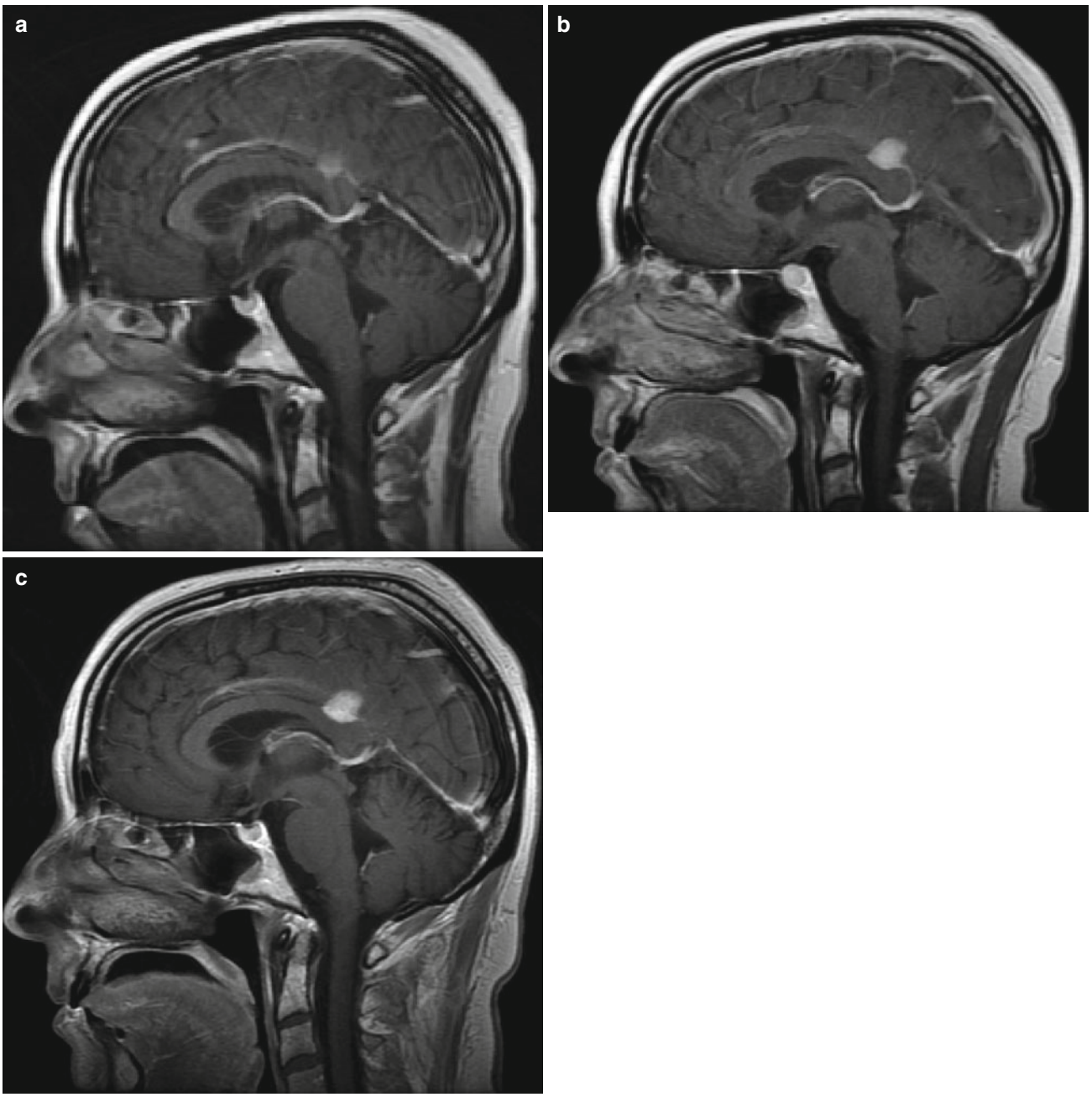

Fig. 3.23 Ipilimumab hypophysitis. Sagittal contrast T1-weighted images obtained before (**a**), during (**b**), and after (**c**) ipilimumab administration in a patient with melanoma. Diffuse homogeneous enlargement of the pituitary gland in (**b**) normalizes in (**c**) after discontinuation of the inciting drug. An enhancing metastasis in the posterior cingulate gyrus in (**a**) increases in (**b**) and then stabilizes in (**c**)

Tuber Cinereum Hamartoma

Tuber cinereum hamartoma is a congenital malformation that can be described as a collection of neurons and glial cells that are located in the tuber cinereum region of the hypothalamus [16]. Tuber cinereum hamartomas are responsible for a third of patients diagnosed with precocious puberty due to excess release of luteinizing hormone-releasing hormone [16, 17]. Although a majority of patients present with symptoms of precocious puberty, seizures are also a common initial presentation. Tuber cinereum hamartoma usually present between the ages of 1 and 3 years old and have no gender predominance [18]. Patients are usually treated medically with hormone suppressants, and surgery is only indicated if medical management fails [16, 18]. Tuber cinereum hamartoma are usually visualized as small, round, nonenhancing lesions on MR and rarely contain cysts or calcium [16].

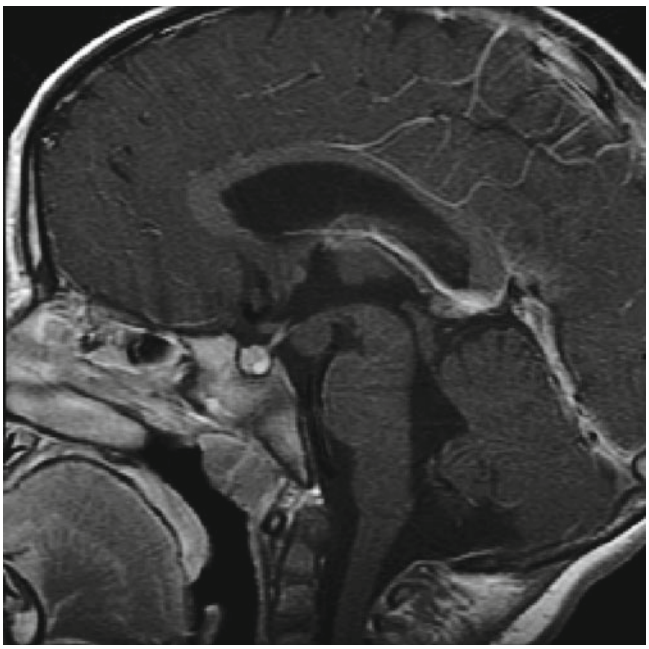

Fig. 3.24 Tuber cinereum hamartoma. Sagittal contrast T1-weighted image shows a nodular lesion located posterior to the infundibulum and anterior to the mammillary bodies along the floor of the anterior third ventricle. The location, lack of enhancement, and isointensity to normal gray matter are diagnostic for a parahypothalamic hamartoma of the tuber cinereum. These are usually found at 10–20 years, more commonly in boys than in girls. Parahypothalamic hamartomas often appear pedunculated and are more likely associated with precocious puberty, whereas intrahypothalamic hamartomas appear sessile, may cause distortion of the floor of the third ventricle, and are more likely associated with gelastic seizures

Langerhans Cell Histiocytosis

Langerhans cell histiocytosis (LCH) is a disease spectrum that evolves as a result of the overproduction of a particular line of dendritic cells that have similar characteristics to Langerhans cells [19]. It is a rapidly progressing disease that can affect virtually any organ within the body and rarely affects the central nervous system (CNS) [19]. The most common CNS manifestation of this disease on MR is a well-circumscribed granuloma located within the sella. Clinical manifestations of this disorder commonly include hormone deficiencies due to invasion of the anterior pituitary [19].

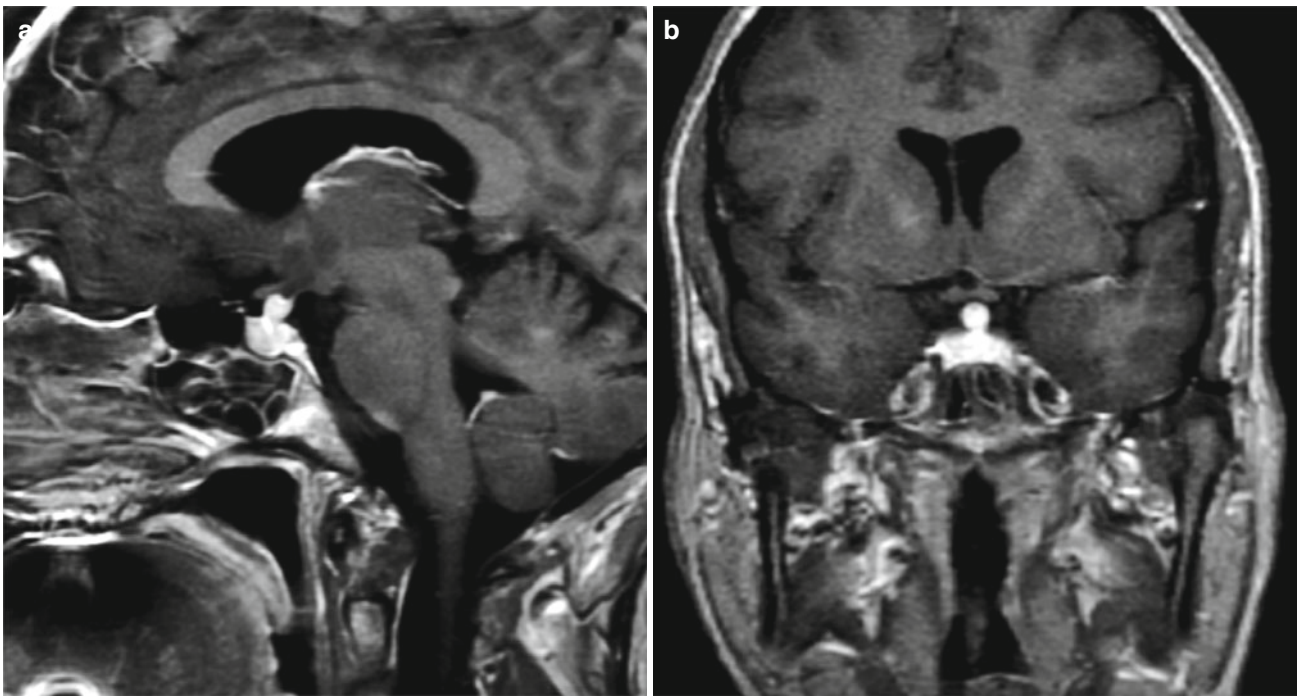

Fig. 3.25 Langerhans cell histiocytosis. Contrast sagittal (**a**) and coronal (**b**) T1-weighted images show thickening of the infundibulum, which is normally less than 3 mm. Loss of the posterior pituitary bright spot (due to vasopressin-containing granules) on pre-contrast images (*not shown*) is consistent with disruption of the normal hypothalamic hypophyseal pathway. One quarter of LCH patients may present with diabetes insipidus. This patient had lytic calvarial lesions consistent with disseminated LCH (*not shown*)

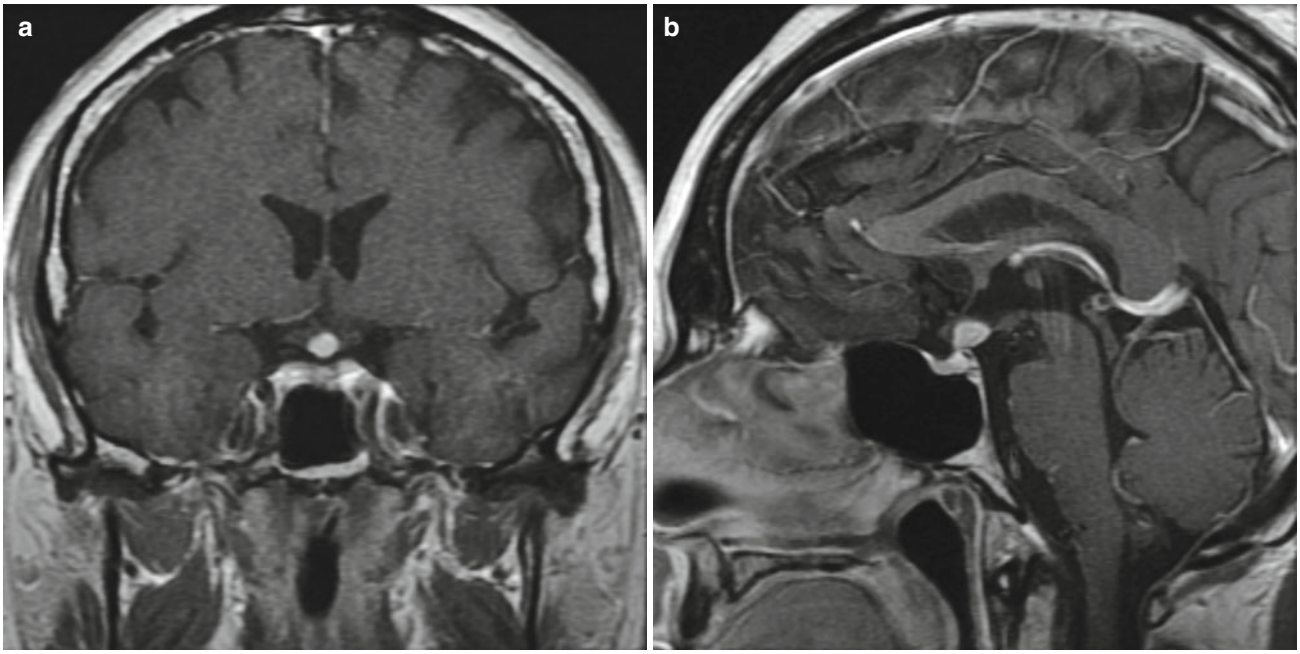

Fig. 3.26 Langerhans cell histiocytosis. Contrast coronal (**a**) and sagittal (**b**) T1-weighted images demonstrate thickening of the infundibulum in a 51-year-old patient (*see* Fig. 3.26). Other possibilities include metastasis, germ cell tumor (in a child), tuberculosis, and sarcoidosis

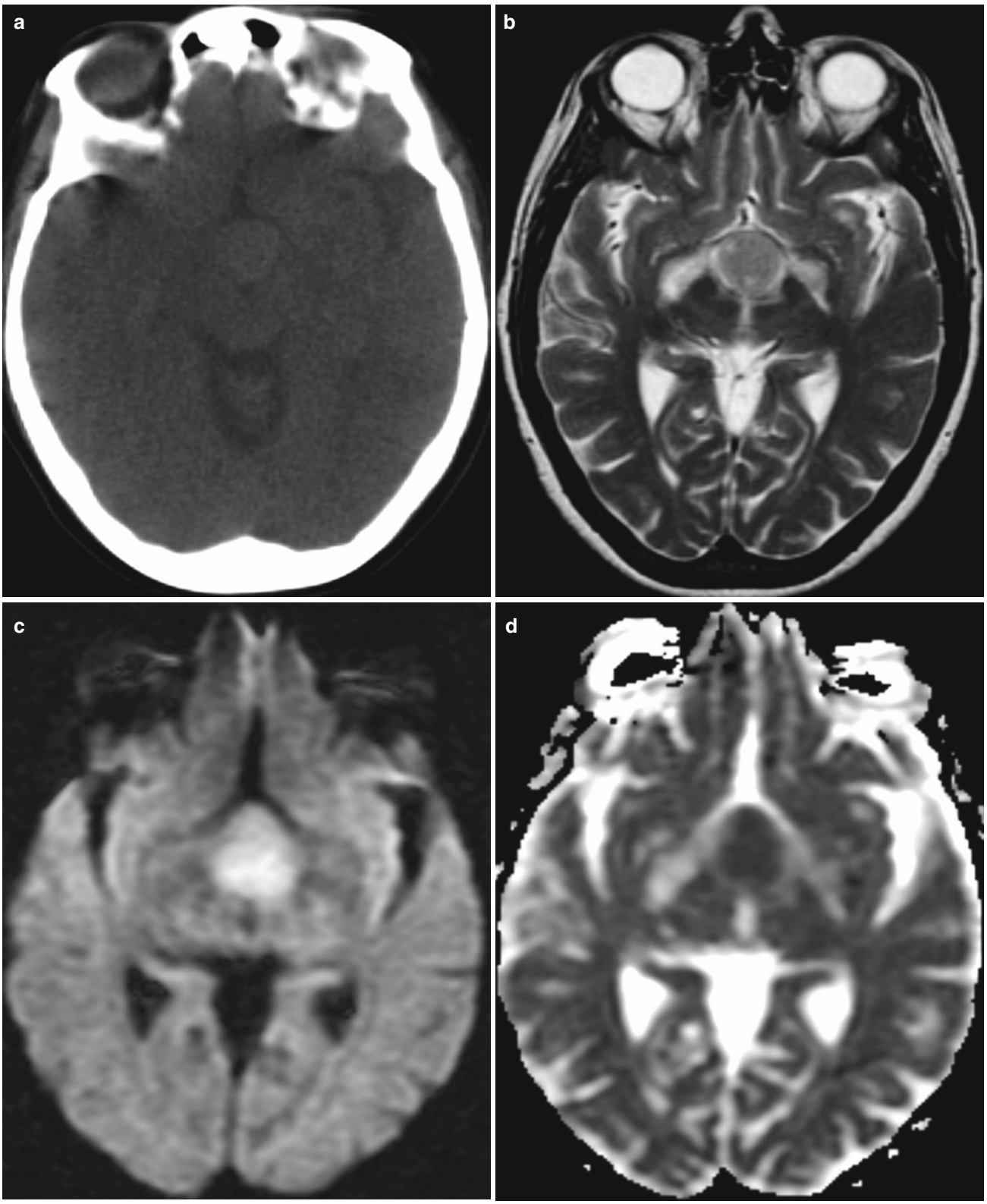

Fig. 3.27 Lymphoma of infundibulum. Axial noncontrast CT (**a**) shows a slightly hyperdense mass of the infundibulum, which is slightly hyperintense on a T2-weighted image (**b**) and diffusion restricted on a diffusion-weighted image (**c**) and apparent diffusion coefficient map (**d**). Contrast axial (**e**) and coronal (**f**) T1-weighted images demonstrate homogeneous enhancement in this lymphoma, where the diffusion restriction is typical for tightly packed cells and high nucleus:cytoplasm ratio, similar to other small, round, blue-cell tumors

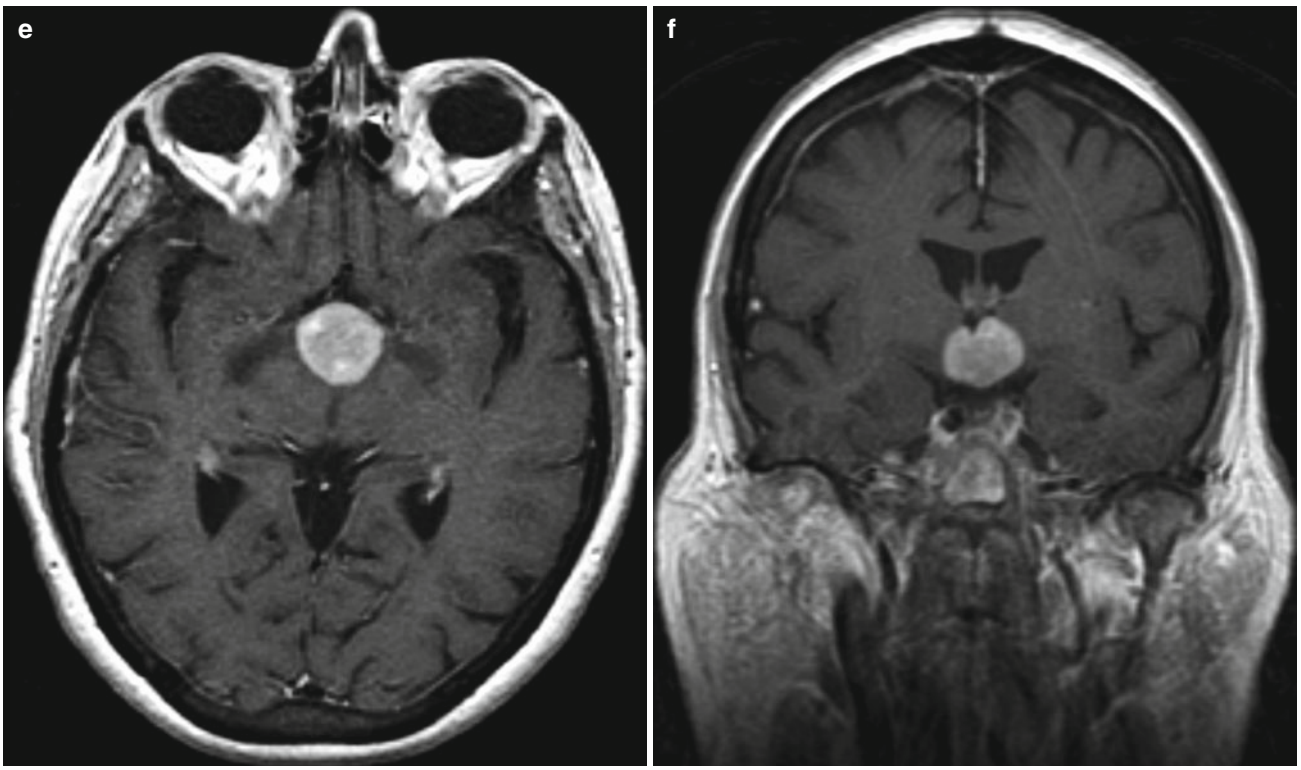

Fig. 3.27 (continued)

Meningioma

A meningioma is a benign slow-growing lesion that arises from the meninges. Meningioma that occurs in the sella/parasellar region of the brain often occur within the midline in the planum sphenoidale or tuberculum sella region [20]. Patients with these lesions usually present with unilateral loss of visual acuity due to compression of optic structures [20]. Surgical resection is only necessary if clinical symptoms are present. Asymptomatic meningioma should be followed by serial imaging. This lesion is most commonly visualized as a dural-based enhancing lesion with the presence of cortical hyperostosis [20, 21].

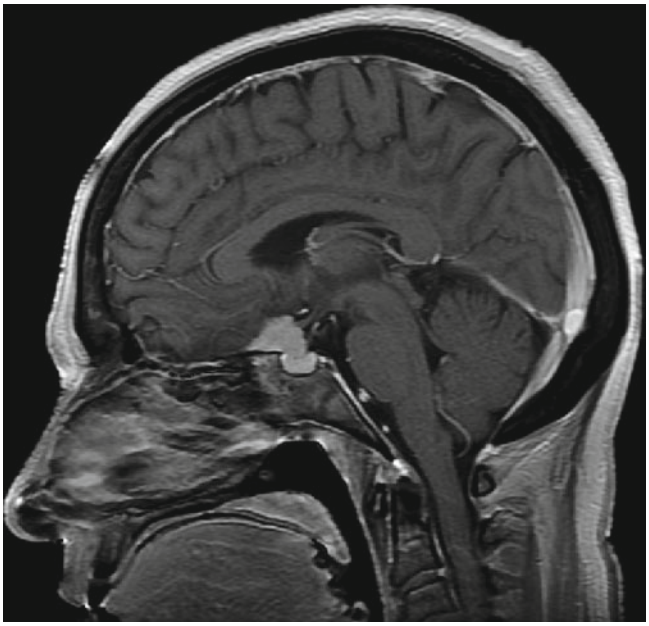

Fig. 3.28 Planum sphenoidale and tuberculum sella meningioma. Contrast sagittal T1-weighted image shows an enhancing extra-axial tumor in the suprasellar cistern with anterior extension and a broad dural base against the planum sphenoidale, and posterior inferior extension over the tuberculum sella toward the sella. Subtle hyperostosis or "blistering" of the dark cortical bone of the planum sphenoidale is diagnostic for a meningioma

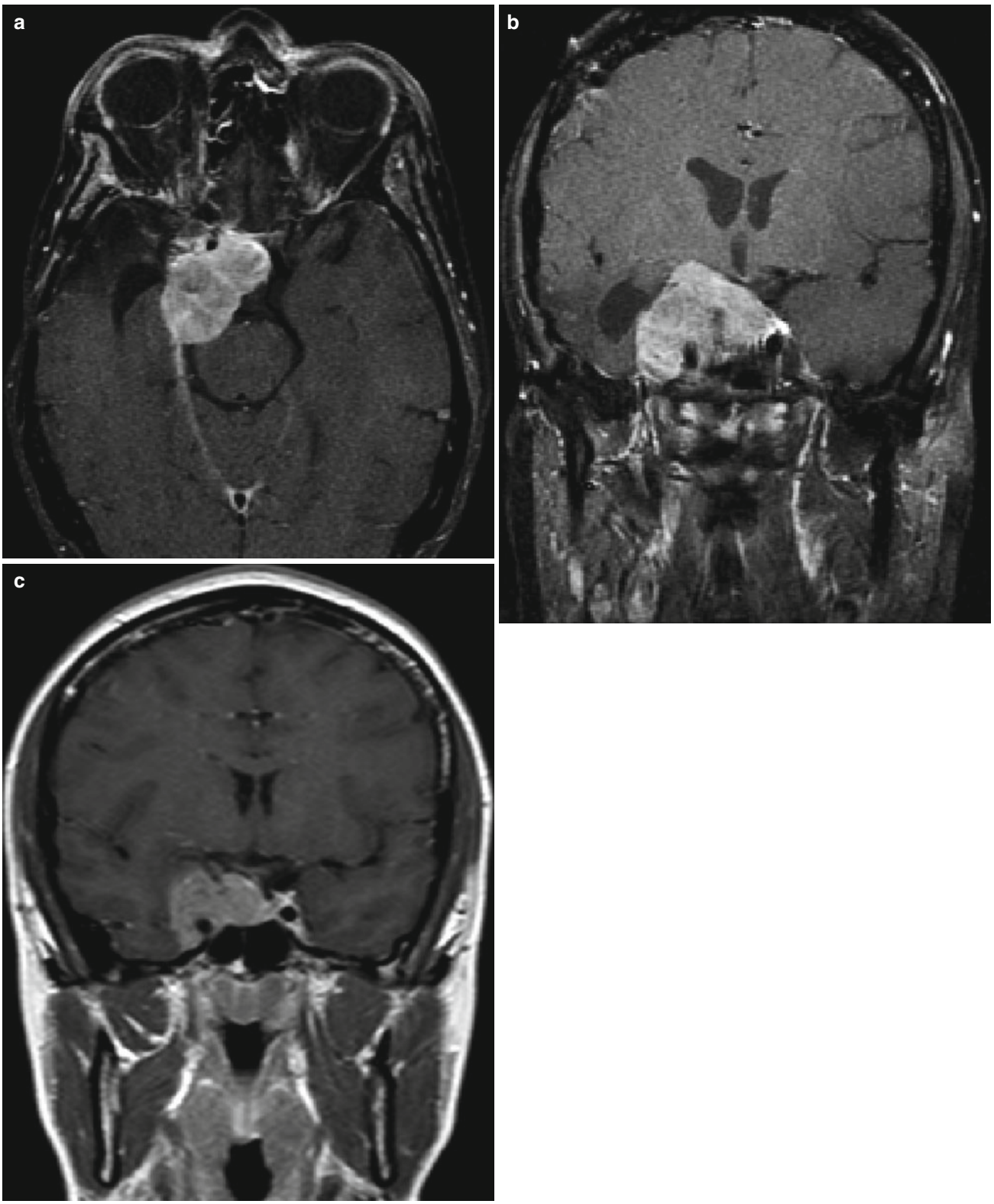

Fig. 3.29 Paracavernous sinus meningioma. Contrast axial (**a**) and coronal T1-weighted images with (**b**) and without (**c**) fat saturation demonstrate an expansile extra-axial enhancing tumor centered in the right cavernous sinus and paracavernous sinus region. There is medial extension into the sella and suprasellar cistern, with mass effect upon the infundibulum, lateral extension into the middle cranial fossa, and posterior extension along the petroclival ligament into the basal and prepontine cisterns

References

1. Johnsen DE, Woodruff WW, Allen IS, et al. MR imaging of the sellar and juxtasellar regions. Radiographics. 1991;11:727–58.
2. Osborne AG. Sella and pituitary. In: Mascarenaz AD, Dearth CL, Kaerli M, editors. Diagnostic imaging: brain. Salt Lake City: Amirsys; 2005. p. 4–7.
3. Bronstein MD, Paraiba DB, Jallad RS. Management of pituitary tumors in pregnancy. Nat Rev Endocrinol. 2011;7:301–10.
4. Osborne AG. Sella and pituitary. In: Mascarenaz AD, Dearth CL, Kaerli M, editors. Diagnostic imaging: brain. Salt Lake City: Amirsys; 2005. p. 20–2.
5. Cottier JP, Destriex C, Brunereau L, et al. Cavernous sinus invasion by pituitary adenoma: MR imaging. Radiology. 2000;215:463–9.
6. Osborne AG. Sella and pituitary. In: Mascarenaz AD, Dearth CL, Kaerli M, editors. Diagnostic imaging: brain. Salt Lake City: Amirsys; 2005. p. 24–6.
7. Berkmann S, Fandino J, Zosso S, et al. Intraoperative magnetic resonance imaging and early prognosis for vision after transsphenoidal surgery for sellar lesions. J Neurosurg. 2011;115:518–27.
8. Byun WB, Kim OL, Kim DS. MR imaging findings of Rathke's cleft cysts: significance of intracystic nodules. AJNR Am J Neuroradiol. 2000;21:485–8.
9. Osborne AG. Sella and pituitary. In: Mascarenaz AD, Dearth CL, Kaerli M, editors. Diagnostic imaging: brain. Salt Lake City: Amirsys; 2005. p. 16–8.
10. Gupta DK, Ojha BK, Sarkar C, et al. Recurrence in craniopharyngiomas: analysis of clinical and histological features. J Clin Neurosci. 2006;13:438–42.
11. Osborne AG. Sella and pituitary. In: Mascarenaz AD, Dearth CL, Kaerli M, editors. Diagnostic imaging: brain. Salt Lake City: Amirsys; 2005. p. 32–4.
12. Shin JL, Asa SL, Woodhouse LJ, et al. Cystic lesions of the pituitary: clinicopathological features distinguishing craniopharyngioma, Rathke's cleft cyst, and arachnoid cyst. J Clin Endocrinol Metabol. 1999;84:3972–82.
13. Kornreich L, Blaser S, Schwarz M, et al. Optic pathway glioma: correlation of imaging findings with the presence of neurofibromatosis. AJNR Am J Neuroradiol. 2001;22:1963–9.
14. Gutenberg A, Larsen J, Lupi I, et al. A radiologic score to distinguish autoimmune hypophysitis from nonsecreting pituitary adenoma preoperatively. AJNR Am J Neuroradiol. 2009;30:1766–72.
15. Osborne AG. Sella and pituitary. In: Mascarenaz AD, Dearth CL, Kaerli M, editors. Diagnostic imaging: brain. Salt Lake City: Amirsys; 2005. p. 40–1.
16. Saleem SN, Said A-HM, Lee DH. Lesions of the hypothalamus: MR imaging diagnostic features. Radiographics. 2007;27:1087–108.
17. Arita K, Ikawa F, Kurisu K, et al. The relationship between magnetic resonance imaging findings and clinical manifestations of hypothalamic hamartoma. J Neurosurg. 1999;91:212–22.
18. Osborne AG. Sella and pituitary. In: Mascarenaz AD, Dearth CL, Kaerli M, editors. Diagnostic imaging: brain. Salt Lake City: Amirsys; 2005. p. 12–4.
19. Grois N, Prayer D, Prosch H, et al. Neuropathology of CNS disease in Langerhans cell histiocytosis. Brain. 2005;128:829–38.
20. Massachusetts General Hospital. Tuberculum sellae meningioma. Accessible at: http://neurosurgery.mgh.harvard.edu/cranialbasecenter/c94.htm. Accessed 1 Dec 2011.
21. Osborne AG. Skull, scalp, and meninges. In: Mascarenaz AD, Dearth CL, Kaerli M, editors. Diagnostic imaging: brain. Salt Lake City: Amirsys; 2005. p. 56–8.